



THE UNIVERSITY *of* EDINBURGH

Edinburgh Research Explorer

Endothelin signalling mediates experience-dependent myelination in the CNS

Citation for published version:

Swire, M, Kotelevtsev, Y, Webb, DJ, Lyons, DA & ffrench-Constant, C 2019, 'Endothelin signalling mediates experience-dependent myelination in the CNS', *eLIFE*, vol. 8, e49493. <https://doi.org/10.7554/eLife.49493>

Digital Object Identifier (DOI):

[10.7554/eLife.49493](https://doi.org/10.7554/eLife.49493)

Link:

[Link to publication record in Edinburgh Research Explorer](#)

Document Version:

Peer reviewed version

Published In:

eLIFE

General rights

Copyright for the publications made accessible via the Edinburgh Research Explorer is retained by the author(s) and / or other copyright owners and it is a condition of accessing these publications that users recognise and abide by the legal requirements associated with these rights.

Take down policy

The University of Edinburgh has made every reasonable effort to ensure that Edinburgh Research Explorer content complies with UK legislation. If you believe that the public display of this file breaches copyright please contact openaccess@ed.ac.uk providing details, and we will remove access to the work immediately and investigate your claim.



1 **Title**

2 Endothelin signalling mediates experience-dependent myelination in the CNS.

3

4 **Authors**

5

6 Matthew Swire^{1,2}, Yuri Kotelevtsev³, David J. Webb⁴, David A. Lyons² and Charles ffrench-Constant¹

7

8 1 MRC Centre for Regenerative Medicine and MS Society Edinburgh Centre, University of Edinburgh,
9 Edinburgh, UK.

10 2 Centre for Discovery Brain Sciences, University of Edinburgh, Edinburgh, UK.

11 3 Centre for Neurobiology and Brain Restoration, Skoltech Institute for Science and Technology,
12 Moscow Region, 143025, Russia.

13 4 British Heart Foundation Centre of Research Excellence, Centre of Cardiovascular Science, Queen's
14 Medical Research Institute, University of Edinburgh, UK.

15

16 **Abstract**

17

18 Experience and changes in neuronal activity can alter CNS myelination, but the signalling pathways
19 responsible remain poorly understood. Here we define a pathway in which endothelin, signalling
20 through the G protein-coupled receptor endothelin receptor B and PKC epsilon, regulates the
21 number of myelin sheaths formed by individual oligodendrocytes in mouse and zebrafish. We show
22 that this phenotype is also observed in the prefrontal cortex of mice following social isolation, and is

23 associated with reduced expression of vascular endothelin. Additionally, we show that increasing
24 endothelin signalling rescues this myelination defect caused by social isolation. Together, these
25 results indicate that the vasculature responds to changes in neuronal activity associated with
26 experience by regulating endothelin levels, which in turn affect the myelinating capacity of
27 oligodendrocytes. This pathway may be employed to couple the metabolic support function of
28 myelin to activity-dependent demand and also represents a novel mechanism for adaptive
29 myelination.

30

31 **Introduction**

32

33 There is increasing evidence that experience regulates CNS myelination. For example, social
34 interactions, sensory stimulation and several forms of learning have been shown to alter white
35 matter and myelin structure in both humans and animal models (Scholz et al., 2009, Makinodan et
36 al., 2012, Liu et al., 2012, Sampaio-Baptista et al., 2013, McKenzie et al., 2014, Etxeberria et al.,
37 2016, Xiao et al., 2016, Hughes et al., 2018). At the level of individual neurons and axons, increasing
38 the level of activity by using optogenetics or chemogenetics enhances the generation of myelin-
39 forming oligodendrocytes and increases the amount of myelin they form (Gibson et al., 2014, Mitew
40 et al., 2018), whilst preventing synaptic vesicular release from axons reduces myelin formation
41 (Hines et al., 2015, Mensch et al., 2015, Koudelka et al., 2016). Together, these findings have led to a
42 new concept of CNS plasticity - adaptive myelination. This concept posits that changes in neuronal
43 activity in response to experience of the extrinsic environment lead to local changes in myelination.
44 Such changes could in turn contribute to the alterations in conduction that underpin CNS neural
45 circuit plasticity (Sampaio-Baptista and Johansen-Berg, 2017, Foster et al., 2019, Suminaite et al.,
46 2019).

47 Exploring this important concept requires that we understand the mechanisms that can link changes
48 in neuronal activity to the regulation of myelination. In addition to the communication between
49 axons of active neurons and the oligodendrocytes that myelinate them, neuronal activity might also
50 affect myelination indirectly in the local area through signals from other glial cells or from vascular
51 cells that can respond to dynamic changes in neuronal activity. Such indirect signalling has been
52 implied by in vitro studies, wherein increased levels of LIF secreted by cultured astrocytes in the
53 presence of neuronal activity enhances myelination (Ishibashi et al., 2006). However, whether the
54 vasculature might relay information about neuronal activity and in turn influence myelination by
55 oligodendrocytes in vivo is not known.

56 Here we set out to test the hypothesis that the vasoactive peptide endothelin (EDN) enables blood
57 vessels to play such a role in indirectly linking activity and myelination. This hypothesis is based on
58 two sets of prior data. First, EDN expression by endothelial cells increases with enhanced blood flow
59 (Yanagisawa et al., 1988, Dancu et al., 2004, Walshe et al., 2005, Pandit et al., 2015), which occurs in
60 response to increased CNS activity. Second, the EDN G-protein coupled receptor (GPCR) endothelin
61 receptor B (EDNRB) enhances myelination in slice cultures (Yuen et al., 2013). Here we show that
62 EDN is expressed by CNS vascular cells, and that this expression lessens in the medial prefrontal
63 cortex following social isolation, which we confirm also leads to impaired cortical myelination.
64 Correspondingly, we show, by manipulating EDNRB signalling in rodent and zebrafish models, that
65 reduced EDN signalling decreases the number of myelin sheaths formed by individual
66 oligodendrocytes in vivo. Finally, we rescue the reduction in myelination associated with
67 environmental social deprivation by intranasal administration of an EDNRB agonist to activate EDN
68 signalling within the CNS. Together our data indicate that the vasculature responds to environmental
69 signals associated with changes in neuronal activity and can, in turn, affect the myelinating capacity
70 of oligodendrocytes in vivo. In this way, we propose a novel mode by which active neurons may
71 regulate oligodendrocyte behaviour and provide a mechanism for adaptive myelination.

72

73 **Results**

74

75 ***The levels of EDN expression in blood vessels are reduced following social isolation***

76 If EDN signalling from CNS blood vessels provides a link between circuit function and myelination,
77 then an initial prediction would be that EDN expression by these vessels will be responsive to
78 extrinsic environmental changes that alter neuronal activity and myelination. To test this prediction,
79 we used a model in which the extrinsic environment has been shown to regulate CNS myelination:
80 social isolation (Liu et al., 2012, Makinodan et al., 2012).

81 Prior work has established that social isolation in mice during a critical period comprising 2 weeks
82 after weaning reduces both the excitability of specific subtypes of pyramidal neurons of the medial
83 prefrontal cortex (mPFC) and oligodendrocyte formation and myelination in the same area (Liu et al.,
84 2012, Makinodan et al., 2012, Yamamuro et al., 2018) We repeated this protocol, confirming the
85 previously-described effect on circuit function by showing that isolated mice spent significantly less
86 time than socially-experienced controls interacting with a novel mouse (figure 1A-C). To quantify the
87 myelination defects in these mice immediately following the isolation period we used a labelling
88 strategy in which oligodendrocyte cell bodies, processes and myelin sheaths are revealed by CNPase
89 immunostaining. The sparsely-myelinated layers II/III of the mPFC, a region myelinated during this
90 isolation period (figure 1D), enabled individual oligodendrocyte morphologies to be analysed for
91 myelin sheath number and length (figure 1D-E, figure 1 - figure supplement 1). Using this approach
92 we showed that individual oligodendrocytes made fewer myelin sheaths (figure 1F-H), although the
93 length of the myelin sheaths formed by oligodendrocytes in these mice was unaffected (figure 1 –
94 figure supplement 2E-F). Further, we found that the isolated mice also generated fewer
95 oligodendrocytes in the mPFC (figure 1 - figure supplement 2C-D). In contrast, social isolation had no

96 effect on myelin sheath number in the visual cortex (figure 1 - figure supplement 3A-B),
97 demonstrating the region-dependent effects of this protocol on myelination.

98 Having validated our social isolation protocol by demonstrating experience-dependent changes in
99 myelination, we next analysed EDN expression in the mPFC. We performed in situ hybridization
100 studies examining the expression of all three EDN ligands (*Edn1-3*) in controls and following
101 isolation. We confirmed robust *Edn1* and *Edn3* mRNA expression in controls, localised to laminin-
102 positive blood vessels, which co-expressed the endothelial/pericyte marker *Pecam1* mRNA (figure
103 2A) (Yanagisawa et al., 1988, Hammond et al., 2014). While previous studies have observed *Edn1*
104 expression also localised to astrocytes following demyelination (Hammond et al., 2014) and
105 microglia (Zhang et al., 2014), here we observed no *Edn1*, *Edn2* or *Edn3* mRNA in S100 β positive
106 astrocytes or IBA1 positive microglia (figure 2 - figure supplement 1A-B), indicating that endothelial
107 cells and/or pericytes are the main source of *Edn* in the healthy mouse brain. Following social
108 isolation, both the number of endothelial cells expressing *Edn1* and *Edn3* mRNA and the expression
109 level of *Edn1* mRNA within each cell was significantly reduced in the mPFC (figure 2B-D, figure 2 -
110 figure supplement 2F-G). However, the vascular area and the number of cells expressing *Pecam1*
111 mRNA were unaffected (figure 2 - figure supplement 2A-E). In contrast to the mPFC, there was no
112 effect of social isolation on *Edn* expression by *Pecam1* cells in the visual cortex (figure 1 - figure
113 supplement 3C). We therefore conclude that the environmental deprivation associated with social
114 isolation reduces vascular *Edn* production in the mouse mPFC.

115

116 ***EDNRB loss reduces the number of myelin sheaths formed by individual oligodendrocytes in vivo***

117 Next, we asked whether a reduction in EDN signalling could potentially contribute to the reduced
118 levels of oligodendrocyte generation and myelination in the isolated mice. To do this, we defined the
119 role of EDN signalling in myelination by performing genetic loss of function experiments to remove
120 the relevant receptor in conditional knockout mice. We targeted the EDN receptor EDNRB due to the

121 high levels of expression in forebrain oligodendrocytes and our own previous work identifying
122 EDNRB as a regulator of myelination in vitro (Yuen et al., 2013, Horiuchi et al., 2017, Marques et al.,
123 2018). We generated a conditional knock out (cKO) using a floxed *Ednrb* mouse line crossed with a
124 line expressing cre recombinase driven by the *Pdgfra* promoter to delete *Ednrb* from
125 oligodendrocytes and their precursor cells through development (figure 3 - figure supplement 1A).
126 Comparison of the number of oligodendrocyte lineage cells in the mPFC in the control (*Pdgfra-*
127 *cre;Ednrb^{wt/wt}*) mice shown in figure1 with EDNRB cKO (*Pdgfra-cre;Ednrb^{flox/flox}*) mice revealed no
128 significant difference in the oligodendrocyte progenitor cell (OPC) or oligodendrocyte generation
129 (figure 3A, figure 3 - figure supplement 1B-D). However, loss of EDNRB in the oligodendroglial
130 lineage significantly reduced the number of myelin sheaths generated by individual oligodendrocytes
131 (figure 3B-D). EDNRB cKO oligodendrocytes demonstrated a 22% reduction in myelin sheath number
132 compared to wild type littermates, but the lengths of the remaining sheaths were unchanged (figure
133 3 - figure supplement 1E-F). A similar effect of EDNRB loss on myelin sheath number was also seen in
134 the visual cortex (figure 1 - figure supplement 3A-B). These experiments show that oligodendroglial
135 EDNRB regulates the number of myelin sheaths formed by individual oligodendrocytes and,
136 strikingly, that this effect of deleting EDNRB was identical to the myelination deficits of individual
137 oligodendrocytes within the mPFC following social isolation in wild-type animals.

138 By contrast, the numbers of oligodendrocytes within the mPFC differs between the two
139 experimental manipulations – reduced by social isolation (figure 1 - figure supplement 2C-D) but not
140 affected by deleting oligodendroglial EDNRB. Given these similarities and difference in the cellular
141 phenotypes of social isolation and EDNRB deletion, we therefore next asked to what extent the
142 changes in behaviour following isolation were phenocopied in the EDNRB cKO mice. Surprisingly,
143 despite the additional effects of social isolation on oligodendrocyte number, the cell type specific
144 loss of EDNRB from the oligodendrocyte lineage was sufficient to cause a significant reduction in the
145 amount of time that cKO mice spent with the novel mouse in the social interaction task, although, as
146 might have been expected, the effect size was smaller than in socially isolated mice, with a 33%

147 reduction following social isolation and 20% following EDNRB CKO as compared to wild type mice
148 (figure 3E, figure 3 - figure supplement 1G-H). We conclude that loss of EDNRB signalling in
149 oligodendrocyte lineage cells phenocopies a specific component of the response of oligodendrocytes
150 to social isolation and that this, in turn, contributes to the behavioural deficits that result from social
151 isolation.

152

153 ***EDNRB signalling enhances myelin sheath number in 3D microfiber cultures***

154 Given that cell-type specific loss of EDNRB results in oligodendrocytes making fewer myelin sheaths
155 per cell, we wanted to ask whether activation of EDNRB signalling in oligodendrocytes might have
156 the complementary effect and promote myelin sheath generation. To do this, we turned to a
157 reductionist in vitro system in which myelination takes place in the absence of confounding
158 influences from other cell types - a 3-dimensional microfiber culture system in which
159 oligodendrocytes form myelin sheaths (Lee et al., 2012a, Bechler et al., 2015). In these cultures we
160 tested both a peptide agonist (BQ2030) and a small molecule antagonist (BQ788) of the receptor.
161 Rat oligodendrocyte precursors were seeded onto poly-l-lactic acid-coated microfibers and allowed
162 to differentiate for 3 days before being treated with BQ2030 or BQ788. We saw a significant increase
163 in the number of myelin sheaths produced by individual oligodendrocytes 11 days later in response
164 to the EDNRB agonist (figure 4A-C). Similar results were obtained with wild type mouse
165 oligodendrocytes (*Pdgfra-cre;Ednrb^{wt/wt}*) while BQ3020 had no effect on EDNRB cKO (*Pdgfra-*
166 *cre;Ednrb^{flox/flox}*) oligodendrocytes (figure 4F-G), confirming the specificity of the agonist for EDNRB.
167 In contrast to the agonist, treatment with the EDNRB antagonist had no effect on myelin sheath
168 number in these cultures (figure 4A-C), as might be expected given the lack of EDN-expressing blood
169 vessel cells, and neither agonist nor antagonist altered sheath length (figure 4D). We conclude from
170 these experiments that the BQ2030 agonist selectively activates EDNRB-mediated signalling
171 pathways in oligodendrocytes that increase myelin sheath number in vitro.

172

173 ***EDNRB promotes myelin sheath formation through Protein Kinase C ϵ .***

174 The observation that we can stimulate myelination by oligodendrocytes in an EDNRB-dependent
175 manner in vitro enabled a biochemical approach to identify the downstream signalling mechanisms
176 by which this was mediated. We therefore next used a forward-phase phosphorylated-protein
177 antibody array of mouse oligodendroglial cultures treated with the EDNRB agonist as an initial
178 screen to identify these downstream pathways. As shown in supplementary file 1, one of the largest
179 changes in protein phosphorylation following EDNRB activation was an increase in the
180 phosphorylation of serine-729 of PKC epsilon, an isozyme of the Protein Kinase C (PKC) family. We
181 confirmed an instructive role of PKC ϵ in two ways. First, we examined myelination in
182 oligodendrocyte microfiber cultures treated with FR 236924, a specific activator of PKC ϵ , which
183 promoted phosphorylation of PKC ϵ at serine-729 (figure 5A) and significantly increased myelin
184 sheath formation (figure 5B-C), similarly to BQ3020. Second, we used zebrafish, due to their
185 amenability for rapid pharmacological treatment and assessment, to test the prediction that the
186 effects on myelination caused by the loss of EDNRB signalling would be rescued by activating the
187 downstream target PKC ϵ in vivo. We obtained a zebrafish line containing a mutation termed rose
188 (*rse*) in one of the orthologues of *Ednrb* (*ednrba*). Analysis of individual oligodendrocytes enabled by
189 sparse labelling of these cells in the fish larvae revealed the same phenotype as in the EDNRB cKO
190 mice; the average number of myelin sheaths formed per oligodendrocyte was reduced by 31% in *rse*
191 homozygous fish compared to wild type controls (figure 5F-G, figure 5 - figure supplement 2A),
192 while sheath length was unaffected (figure 5 -figure supplement 2B-C). As predicted, activation of
193 PKC ϵ by FR236924 treatment from 3-4 days post fertilisation, rescued myelin sheath number in *rse*
194 homozygous fish (figure 5D-G). This result confirms a role for PKC ϵ downstream of EDNRB in the
195 regulation of myelin sheath number in vivo.

196

197 ***Increasing EDNRB signalling rescues the reduction in myelin sheath number resulting from social***
198 ***isolation.***

199 Our results have shown that social isolation decreases the levels of EDN expression in the CNS
200 vasculature, and that EDNRB signalling in oligodendrocytes influences myelin sheath number. It
201 follows that the decreased EDN signalling is likely contributing to the reduction in myelin sheath
202 numbers seen in the prefrontal cortex following social isolation. If so, then we would predict that
203 activation of EDNRB in vivo in the prefrontal cortex would rescue the myelin sheath phenotype
204 associated with social isolation. To test this we used intranasal administration, a technique shown to
205 enable the delivery of peptides into the CNS (Scafidi et al., 2014, Crowe et al., 2018) to introduce the
206 EDNRB agonist BQ3020. Socially isolated mice were given 1µg BQ3020 twice daily intranasal
207 administration or saline for a period of 10 days from postnatal day 21 to 31 (during the period of
208 isolation), and perfused at postnatal day 35 for analysis of mPFC myelination as above. Importantly,
209 we confirmed that the daily handling involved in this protocol did not negate the effects of social
210 isolation by showing that the sheath numbers in the control isolated mice administered saline had
211 the same reduction in sheath numbers as completely isolated animals (figure 6B and D-E). Strikingly,
212 and in keeping with our prediction, 10 days of BQ3020 treatment to socially-isolated animals
213 rescued the myelination phenotype normally seen in these mice, with a 20% increase in the number
214 of myelin sheaths formed by mPFC oligodendrocytes in treated animals, meaning that the sheath
215 numbers were now not significantly different to wild-type animals housed in groups (figure 6D-E).

216

217 **Discussion**

218

219 Here we identify a novel signalling pathway in which the oligodendroglial G-protein coupled receptor
220 EDNRB regulates myelin sheath number and the response of oligodendrocytes to social experience

221 (figure 6 - figure supplement 21A). We studied mice following a previously established experimental
222 manipulation in which early postnatal social isolation leads to a reduction in the number of myelin
223 sheaths formed by individual oligodendrocytes in the medial prefrontal cortex (mPFC) of mice. We
224 showed that isolated animals have reduced EDN mRNA expression in the blood vessels of the mPFC.
225 We found that perturbing endothelin signalling in oligodendroglia by a conditional knockout of the
226 EDN receptor EDNRB phenocopies the reduced number of sheaths seen in the isolated animals. In
227 turn intranasal administration of an EDNRB agonist during the period of isolation rescues the effects
228 of social deprivation on myelination. Together with additional experiments in cell culture and
229 zebrafish, which identified the protein kinase C (PKC) epsilon isoform as being activated downstream
230 of EDNRB to regulate myelination by oligodendrocytes, our loss- and gain-of-function experiments
231 demonstrate a role for endothelin signalling in regulating the number of myelin sheaths formed by
232 individual oligodendrocytes.

233 Our work provides evidence for the importance of the interaction between the vasculature and
234 oligodendroglia during myelination per se, extending observations indicating that the vasculature
235 can influence earlier stages of the oligodendrocyte lineage. For example, during development,
236 oligodendrocyte progenitor cells use blood vessels as a scaffold to migrate along (Tsai et al., 2016).
237 Once in place, local oxygen levels influence their differentiation into oligodendrocytes, stalling the
238 process when levels are low. Only when an adequate oxygen supply is established are the cells able
239 to differentiate and begin the process of myelination (Yuen et al., 2014). Here, we demonstrate a
240 third role – the regulation of myelination itself through the control by EDN of myelin sheath number
241 by individual differentiated oligodendrocytes. Such a role is potentially important, as it provides an
242 indirect mechanism by which the regulation of myelination in the CNS might be linked to levels of
243 neuronal activity. A key function of myelin is the provision of metabolic substrates to the underlying
244 axon via specific transporters within the inner layer of the sheath (Fünfschilling et al., 2012, Lee et
245 al., 2012b, Meyer et al., 2018). These substrates drive ATP production within the axon, so providing a
246 source of energy at some distance from the cell body as required to sustain axonal activity. Prior

247 work has implicated that NMDA receptor activation in oligodendrocytes following glutamate release
248 by active axons in relaying the need for metabolic support of axons to oligodendrocytes (Saab et al.,
249 2016). We now propose that an increase in EDN production by endothelial cells, as predicted to
250 occur in the presence of increased blood flow or hypoxia, will increase myelin sheath generation by
251 local oligodendrocytes and so provide a further means of linking energy supply and demand.
252 Changes in blood flow and hypoxaemia are associated with increased cortical activity (forming the
253 basis of the BOLD signal detected by fMRI). Therefore, an EDN-mediated pathway driving an increase
254 in myelination is a plausible mechanism for ensuring that the metabolic demands of active axons are
255 met. Further work examining the effect of EDNRB loss in oligodendrocytes on axonal function and
256 viability in ageing are required to test this further.

257 A second important implication of our study relates to the emerging concept of adaptive
258 myelination. This concept argues that myelination in the CNS is plastic, and regulated by differing
259 codes of activity, each eliciting different effects on myelination that in turn alter circuit function. This
260 hypothesis therefore proposes that adaptive myelination represents a form of neural plasticity that
261 could, like synaptic plasticity, enable the brain to modify circuit function in response to experience-in-
262 other words, to adapt. However, this hypothesis remains to be fully explored, and a key requirement
263 for these experiments is the identification of the mechanisms that link changes in activity patterns
264 following experience to the changes in oligodendrocyte number and/or sheath formation that could
265 alter circuit function. Prior work has identified a direct role for axon-derived signals in regulating
266 myelination. We now identify a mechanism by which the effects of activity could lead to an
267 increased number of myelin sheaths through indirect signalling via the vasculature. Our findings
268 showing that social isolation reduces endothelial EDN expression, that an oligodendroglial-specific
269 deletion of the relevant EDNRB receptor phenocopies the myelination defect caused by social
270 isolation, and that an EDNRB agonist rescues the myelination defect of individual oligodendrocytes
271 in the mPFC together argue strongly for a role of vascular EDN synthesis in mediating such indirect
272 effects. Our results do not however imply that changes in EDN signalling are solely responsible for

273 the effects of social isolation on myelination. It is clear, for example, that social isolation can affect
274 oligodendrocyte number, a feature that does not appear to be controlled by EDN in the healthy
275 nervous system. Other pathways could contribute to this aspect of adaptive myelination. Such
276 potential pathways are BDNF signalling via oligodendroglia TrkB (Geraghty et al., 2019, Gibson et al.,
277 2019) and glutaminergic signalling via AMPAR-mediated effects on newly differentiating
278 oligodendrocytes (Kougioumtzidou et al., 2017). Further work manipulating EDN expression
279 specifically in endothelial cells during social isolation is required to explore this.

280

281 Based on recent live imaging studies showing that myelin sheath numbers in cortical
282 oligodendrocytes remain largely stable throughout life (Hill et al., 2018, Hughes et al., 2018), we
283 propose that any endothelin-mediated regulation of sheath number is likely to occur around the
284 birth of each newly formed oligodendrocyte. The continuous generation of oligodendrocytes in the
285 adult CNS, itself increased by activity-related signals ensures that dynamic regulation of endothelin
286 signalling from the vasculature has the capacity to play a role in adaptive myelination throughout
287 life.

288 How though might new myelin sheaths formed by individual oligodendrocytes in response to EDN
289 signalling enhance circuit function the cortex? By linking metabolic demand to metabolic support for
290 axons in regions of high activity (as discussed above), EDN signalling in cortical oligodendrocytes
291 could play a central role in enhancing the ability of the axon to sustain higher levels of energy-
292 requiring conduction, so enabling changes in circuit function. An intriguing possibility suggested by a
293 comparison of gene expression in cortical oligodendroglia and spinal cord oligodendroglia showing
294 higher levels of expression of EDNRB in the former (Horiuchi et al., 2017, Marques et al., 2018), is
295 that these cortical oligodendrocytes are specialised for this role linking metabolic demand to
296 support. By contrast, oligodendrocytes in white matter might be more specialised for rapid axonal
297 conduction. Further work examining oligodendrocyte heterogeneity between grey matter and white

298 matter regions of the CNS will be required to test this. Another way in which additional myelin
299 sheaths might impact circuit function is the addition of sheaths to axons in the cortex that are
300 discontinuously and sparsely myelinated (Tomassy et al., 2014, Hill et al., 2018, Hughes et al., 2018).
301 The resulting effects on conduction velocity resulting from short stretches of axons now supporting
302 rapid saltatory conduction could, as has been suggested elsewhere, enable activity-dependent
303 myelination to have a role in signal synchrony (Seidl et al., 2010, Seidl et al., 2014, Freeman et al.,
304 2015, Baraban et al., 2016, Timmler and Simons, 2019). However, such a model requires a very
305 precise link between axonal selection and myelination, and the precision required may be difficult to
306 achieve with a diffusible vascular-derived signal.

307 Our findings on the role of EDN in myelination complement other investigations demonstrating a
308 role of astrocytic EDN hindering oligodendrocyte differentiation during remyelination (Hammond et
309 al., 2014, Hammond et al., 2015). In agreement with this observation, our global EDNRB mutant
310 zebrafish were found to have an increased number of oligodendrocytes (figure 5 - figure supplement
311 1). Together previous studies and ours suggest that EDN signalling plays two roles, indirectly
312 inhibiting oligodendrocyte formation, but, promoting myelin sheath formation once differentiation
313 has occurred. At apparent odds with this conclusion, conditional loss of EDNRB from
314 oligodendrocyte progenitors had no effect on remyelination; having deleted OPC EDNRB from adult
315 mice 3 days prior to demyelination of the external capsule, Hammond and colleagues observed that
316 the percentage of remyelinated axons, assessed by electron microscopy, was unchanged 14 days
317 after injury (Hammond et al., 2015). However, this divergence may result from the different
318 microenvironments of developmental myelination and remyelination or from intrinsic differences
319 between cortical and white matter oligodendrocytes, as discussed above, and further studies
320 examining grey matter remyelination are required to resolve the point.

321 The conclusion that EDN has contrasting effects on oligodendrocyte formation and on myelination
322 highlights that these two steps in oligodendrocyte development are regulated independently. This in

323 turn has important implications for the development of regenerative therapies for the progressive
324 neurodegenerative phase of the demyelinating disease Multiple Sclerosis (MS). Current strategies
325 seeking to re-purpose FDA approved drugs to enhance remyelination, and so restore the
326 neuroprotective effect of the myelin sheath to the axon, have focused largely on the differentiation
327 step from precursor cell to oligodendrocyte, with one screen using micropillar arrays to examine the
328 later stage of wrapping (Mei et al., 2014). None however specifically examine the key final step-
329 formation of the sheath itself. Neuropathological studies of MS lesions revealing pre-myelinating
330 oligodendrocytes unable to complete remyelination suggest for that failure of this final step may
331 contribute to pathology. These findings emphasise that the already differentiated oligodendrocyte
332 represents a possible target for remyelination strategies in MS, a conclusion reinforced by recent
333 papers using Carbon14 dating, electron microscopy or snRNA seq of post mortem human MS
334 material providing evidence that pre-existing adult oligodendrocytes contribute to repair (Duncan et
335 al., 2018, Jäkel et al., 2019, Yeung et al., 2019). Strategies to identify targets within pathways such as
336 that activated by EDNRB that promote sheath formation directly will therefore be an important
337 addition to the current approaches being taken in drug discovery for progressive multiple sclerosis.

338

339 **Acknowledgments**

340 We would like to thank Dr Marie Bechler for help with microfiber cultures and past and present
341 members of the French-Constant, Lyons, Williams and Miron labs for technical assistance and
342 helpful discussions. We thank the University of Edinburgh facilities for animal husbandry and
343 support. This work was supported by a MS Society Research Grant PhD studentship (Grant
344 Reference 950), a Wellcome Trust Senior Investigator Award to CffC and a Wellcome Trust Senior
345 Research Fellowship (102836/Z/13/Z) to DL.

346

347 **Competing interests**

348 No competing interests declared

349

350 **Figure legends**

351 **Figure 1 – Social isolation in mice reduces layer II/III medial prefrontal cortex oligodendrocyte**
352 **myelin sheath number.**

353 A Timeline for social isolation experiment. At postnatal day 21 male mice were housed in a social
354 environment containing 3-5 mice or on their own in isolation. Mice were analysed at P35.

355 B Schematic of social interaction assay. Mice were recorded for 5 minutes exploring an arena
356 containing 2 identical wire mesh containers: one container housed an unrelated male wild type
357 mouse (social zone), while the other remained empty (non-social zone).

358 C Time spent within 2.5cm of non-social container: Grouped 37.58 seconds \pm 8.683 n=12, Isolated
359 45.59 \pm 36.28 n=9 and social container: Grouped 110.7 seconds \pm 21.71 n=12, Isolated 74.24 seconds
360 \pm 37.07 n=9 (mean \pm standard deviation). Unpaired T-test p=0.0107.

361 D Coronal section of mouse prefrontal cortex stained for CNPase and nuclei. Layers II/III of the
362 medial prefrontal cortex outlined by dashed box. Scale bars = 100 μ m.

363 E Layer II/III oligodendrocyte stained for CNPase and MBP.

364 F Representative images of medial prefrontal cortex oligodendrocytes stained for CNPase.

365 G Mean number of myelin sheath formed by oligodendrocytes per mouse. Grouped 47.66 \pm 1.015
366 n=7 mice, Isolated 37.11 \pm 0.6425 n=4 mice (mean \pm standard error). Mann-Whitney test, p=0.0106.

367 H Pooled data for number of myelin sheaths formed by layer II/III medial prefrontal cortex
368 oligodendrocytes. Grouped 47.80 ± 7.289 n=49 cells from 7 mice, Isolated 37.11 ± 5.202 n=28 cells
369 from 7 mice (mean \pm standard deviation). Mann-Whitney test, $p < 0.001$.

370 **Figure 2 – Social isolation reduces vascular endothelin expression.**

371 A *Edn1* and *Edn3* mRNA expression in laminin positive and CD31 positive blood vessels as revealed
372 by RNAScope in situ hybridisation.

373 B Representative images of *Edn1* and *Pecam1* mRNA expression in the mPFC.

374 C Quantification of the number of *Edn1* expression *Pecam1* positive endothelial cells. Grouped
375 0.8033 ± 0.04411 n=4 mice, Isolated 0.5074 ± 0.05412 n=5 mice (mean \pm standard error). Mann-
376 Whitney test, $p=0.0159$.

377 D Quantification of the mean *Edn1* mRNA molecules expressed by *Pecam1* positive cells per mouse.
378 Grouped 12.29 ± 3.312 n=5 mice, Isolated 4.673 ± 0.4059 n=4 mice (mean \pm standard error). Mann-
379 Whitney test, $p=0.0159$.

380

381 **Figure 3 – Loss of oligodendroglial EDNRB reduces myelin sheath number and reduces sociability.**

382 A Quantification of CNP positive cells in medial prefrontal cortex layers II/III: Wild type 7709 ± 378.7
383 n=5 mice, EDNRB CKO 7288 ± 1054 n=4 mice (mean \pm standard error) and layer V: Wild type $18879 \pm$
384 1559 n=9 mice, EDNRB CKO 21016 ± 2878 n=3 mice (mean \pm standard error). Mann Whitney test,
385 layer II/III $p= 0.9048$, layer V $p= 0.3527$.

386 B Representative images of medial prefrontal cortex oligodendrocytes stained for CNPase. Scale bar
387 = 20 μ m.

388 C Mean number of myelin sheath formed by oligodendrocytes per mouse. Wild type 47.66 ± 1.015
389 $n=7$ mice, EDNRB CKO 37.39 ± 1.099 $n=4$ mice (mean \pm standard error). Mann-Whitney test,
390 $p=0.0106$.

391 D Pooled data for number of myelin sheaths formed by layer II/III medial prefrontal cortex
392 oligodendrocytes. Wild type 47.80 ± 7.289 $n=49$ cells from 7 mice, EDNRB CKO 37.39 ± 7.208 $n=28$
393 cells from 7 mice (mean \pm standard deviation). Mann-Whitney test, $p < 0.001$.

394 E Time spent within 2.5cm of non-social container: Wild type 37.58 seconds \pm 8.683 $n=12$, EDNRB
395 CKO 41.06 ± 21.29 $n=14$ and social container: Wild type 110.7 seconds \pm 21.71 $n=12$, EDNRB CKO
396 88.39 seconds \pm 25.79 $n=14$ (mean \pm standard deviation). Unpaired T-test $p=0.0267$.

397

398 **Figure 4 – EDNRB enhances myelin sheath number in vitro.**

399 A Representative images of MBP positive oligodendrocytes in microfiber culture. Scale bar = 50 μ m.

400 B Mean number of myelin sheaths formed by rat oligodendrocytes on microfibers per independent
401 culture preparation. Control 7.253 ± 0.4258 $n=8$ independent cultures, BQ3020 11.21 ± 0.58635 $n=7$
402 independent cultures, BQ788 6.026 ± 0.7046 (mean \pm standard error) $n=4$ independent cultures. 1-
403 way ANOVA with Tukey's post hoc test.

404 C Pooled data for number of myelin sheaths formed by rat oligodendrocytes on microfibers. Control
405 7.194 ± 3.544 $n=160$ cells from 8 independent cultures, BQ3020 11.25 ± 4.420 $n=127$ from 7
406 independent cultures, BQ788 6.024 ± 3.059 $n=85$ cells from 4 independent cultures (mean \pm
407 standard deviation). Kruskal-Wallis test, with Dunns post hoc.

408 D Frequency distribution of myelin sheath lengths formed on microfibers.

409 E qPCR for EDNRB from mouse oligodendrocyte cultures. Wild type 1.292 ± 0.04933 n=4
410 independent cultures, EDNRB CKO 0.5958 ± 0.1117 n=4 independent cultures, BQ788 6.026 ± 0.7046
411 (mean \pm standard error). Unpaired T-test p=0.0013.

412 F Mean number of myelin sheaths formed by mouse oligodendrocytes on microfibers per
413 independent culture preparation. Wild type 6.18 ± 0.2082 n=5 independent cultures, Wild type +
414 BQ3020 9.732 ± 0.07548 n=4 independent cultures, EDNRB CKO 5.380 ± 0.4181 n=5 independent
415 cultures, EDNRB CKO + BQ3020 5.989 ± 0.6125 n=4 independent cultures (mean \pm standard error). 1-
416 way ANOVA.

417 G Pooled data for number of myelin sheaths formed by mouse oligodendrocytes on microfibers.
418 Wild type 6.138 ± 1.499 n=65 cells from 5 independent cultures, Wild type + BQ3020 9.705 ± 2.575
419 n=44 from 4 independent cultures, EDNRB CKO 5.345 ± 1.824 n=65 cells from 5 independent cultures,
420 EDNRB CKO + BQ3020 5.955 ± 2.632 n=44 cells from 4 independent cultures (mean \pm standard
421 deviation). Kruskal-Wallis test, with Dunns post hoc.

422

423 **Figure 5 – Protein kinase C epsilon is downstream of EDNRB to regulate myelin sheath number.**

424 A Western blot images of rat oligodendrocytes treated with EDNRB agonist BQ3020 and PKC ϵ
425 agonist FR 236924 for 15 minutes. Antibodies used: Phosphorylated PKC ϵ S729 and loading control
426 GAPDH.

427 B Mean number of myelin sheaths formed by rat oligodendrocytes on microfibers per experiment.
428 Control 5.959 ± 0.4708 n=4, FR 236924 9.542 ± 0.3614 n=3 (mean \pm standard error). Unpaired T-test
429 p=0.0024.

430 C Pooled data for number of myelin sheaths formed by rat oligodendrocytes on microfibers. Control
431 5.952 ± 2.525 n=62 cells from 4 experiments, FR 236924 9.542 ± 4.016 n=48 from 3 experiments
432 (mean \pm standard deviation). Mann-Whitney test, p= <0.001.

433 D Schematic for zebrafish larvae treatment with FR 236924.

434 E Representative images of 4 dpf zebrafish larvae treated with DMSO control or FR 236924. Scale bar
435 = 500 μ m.

436 F Representative images of mbp:EGFP-CAAX oligodendrocytes in 4 dpf zebrafish larvae. Scale bar =
437 10 μ m.

438 G Pooled data for number of myelin sheaths formed by zebrafish oligodendrocytes. EDNRB Het
439 12.35 ± 3.746 n=20 cells, EDNRB Hom 9.073 ± 2.229 n=41 from 4 experiments, EDNRB Het + FR
440 236924 13.5 ± 3.098 n=22 cells from 5 experiments, EDNRB Hom + FR 236924 14 ± 4.807 n=19 cells
441 (mean \pm standard deviation). 1-way ANOVA.

442

443 **Figure 6 – Intranasal administration of an EDNRB agonist rescues the myelin sheath number**
444 **reduction caused by social isolation.**

445 A Timeline for the intranasal experiment. At postnatal day 21 male mice were housed on their own
446 in isolation. Mice were given 2 daily administrations of saline or EDNRB agonist BQ3020 from P21-
447 P30. Mice were analysed at P35.

448 B Time spent within 2.5cm of non-social container: Saline 57.42 seconds ± 24.44 n=12, BQ3020 41.44
449 ± 17.43 n=17 and social container: Saline 75.82 seconds ± 13.26 n=12, BQ3020 84.96 seconds \pm
450 37.20 n=17 (mean \pm standard deviation). T-test.

451 C Quantification of CNP positive cells in medial prefrontal cortex layers II/III: Saline 7278 ± 1165 n=3
452 mice, BQ3020 9142 ± 713.3 n=3 mice (mean \pm standard error) and layer V: Saline 17114 ± 2750 n=5
453 mice, BQ3020 16154 ± 1980 n=4 mice (mean \pm standard error).

454 D Mean number of myelin sheath formed by oligodendrocytes per mouse. Saline 39.54 ± 0.4301 n=4
455 mice, BQ3020 47.29 ± 1.687 n=4 mice (mean \pm standard error). Mann-Whitney test, p=0.0286.

456 E Pooled data for number of myelin sheaths formed by layer II/III medial prefrontal cortex
457 oligodendrocytes. Saline 39.54 ± 6.973 n=28 cells from 4 mice, BQ3020 47.29 ± 10.18 n=28 cells from
458 7 mice (mean \pm standard deviation). Mann-Whitney test, p=0.0019.

459

460 **Figure 1- figure supplement 1 – Z-stack through a CNPase positive oligodendrocytes.**

461 A full maximum intensity projection of a complete a layer II/III oligodendrocytes in mouse cortex
462 stained for CNPase followed by 0.5 μ m slices. Tracing the fine processes through each slice enables
463 assessment of the myelin sheaths formed by individual oligodendrocytes.

464

465 **Figure 1- figure supplement 2 – Social isolation reduces oligodendrocyte generation.**

466 A Distance travelled by mice during 5 minutes of exploration of the social interaction assay. Grouped
467 15.48 meters ± 3.326 n=12 mice, Isolated 16.15 meters ± 3.57 n=9 mice (mean \pm standard deviation).

468 B Maximum speed travelled by mice during 5 minutes of exploration of the social interaction assay.
469 Grouped 0.2433 ± 0.04117 n=12 mice, Isolated 0.2619 meters ± 0.02792 n=9 mice (mean \pm standard
470 deviation).

471 C Quantification of CNP positive cells in medial prefrontal cortex layers II/III: Grouped 7709 ± 378.7
472 n=5 mice, Isolated 4738 ± 385.7 n=4 mice (mean \pm standard error).

473 D Quantification of CNP positive cells in medial prefrontal cortex layer V: Grouped 18879 ± 1559 n=9
474 mice, Isolated 13099 ± 1052 n=9 mice (mean \pm standard error).

475 E Mean myelin sheath length formed by oligodendrocytes per mouse. Grouped $46.10 \mu\text{m} \pm 2.485$
476 n=7 mice, Isolated $51.48 \mu\text{m} \pm 4.08$ n=4 mice (mean \pm standard error).

477 F Frequency distribution of myelin sheath lengths.

478

479 **Figure 1- figure supplement 3 – Loss of oligodendroglial EDNRB reduces myelin sheath number in**
480 **the visual cortex where social isolation does not affect myelination or *Edn1* expression.**

481 A Mean number of myelin sheath formed by oligodendrocytes per mouse. Wild type 52.57 ± 1.270
482 $n=4$ mice, EDNRB CKO 42.39 ± 1.487 $n=4$ mice, Isolated 50.32 ± 0.8755 $n=4$ mice (mean \pm standard
483 error). Mann-Whitney test, $p=0.0106$. Kruskal-Wallis test, with Dunns post hoc.

484 B Pooled data for number of myelin sheaths formed by layer II/III visual cortex oligodendrocytes.
485 Grouped 52.57 ± 8.779 $n=28$ cells from 4 mice, EDNRB CKO 42.39 ± 7.213 $n=28$ cells from 4 mice,
486 Isolated 50.32 ± 5.716 $n=28$ cells from 4 mice (mean \pm standard deviation). Kruskal-Wallis test, with
487 Dunns post hoc.

488 C Quantification of the number of *Edn1* expressing *Pecam1* positive cells. Grouped 0.6449 ± 0.02814
489 $n=4$ mice, Isolated 0.63535 ± 0.02120 $n=4$ mice (mean \pm standard error). Mann-Whitney test.

490

491 **Figure 2- figure supplement 1 – EDN mRNA is not expressed in astrocytes and microglia.**

492 Expression of *Edn1*, *Edn2* and *Edn3* in S100 β positive astrocytes and IBA1 positive microglia. A
493 RNAScope in situ hybridisation for *Edn1*, *Edn2* and *Edn3* mRNA in the mouse medial prefrontal
494 cortex stained for S100 β positive astrocytes. Note that S100 β positive cells are negative for *Edn1* and
495 *Edn3* mRNA while positive *Edn* signal can be seen in S100 β negative cells.

496 B RNAScope in situ hybridisation for *Edn1*, *Edn2* and *Edn3* mRNA in the mouse medial prefrontal
497 cortex stained for Iba1 positive microglia. Note that Iba1 positive cells are negative for *Edn1* and
498 *Edn3* mRNA while positive *Edn* signal can be seen in Iba1 negative cells.

499

500 **Figure 2 - figure supplement 2 – Social isolation does not affect medial prefrontal cortex**
501 **vasculature.**

502 A Representative images of medial prefrontal cortex vasculature staining for PECAM1.

503 B Quantification of PECAM1 area in medial prefrontal cortex layer II/III: Grouped $2.468 \% \pm 0.3156$
504 $n=6$ mice, Isolated 2.086 ± 0.13 $n=6$ mice (mean \pm standard error). Mann-Whitney test.

505 C Quantification of number of *Pecam1* mRNA expressing cells per field of view. Grouped 9 ± 0.5888
506 $n=4$ mice, Isolated 8.44 ± 1.162 $n=4$ mice (mean \pm standard error). Mann-Whitney test.

507 D Quantification of the number of *Pecam1* mRNA molecules. Grouped 13.47 ± 6.204 $n=77$ cells from
508 4 mice, Isolated 10.89 ± 5.02 $n=92$ cells from 5 mice (mean \pm standard deviation). Mann-Whitney
509 test, $p= 0.002$.

510 E Quantification of the number of *Pecam1* mRNA molecules per mouse. Grouped 13.53 ± 1.305 $n=4$
511 mice, Isolated 10.48 ± 1.018 $n=5$ mice (mean \pm standard error). Mann-Whitney test.

512 F Quantification of the number of *Edn1* mRNA molecules in *Pecam1* positive endothelial cells.
513 Grouped 12.08 ± 9.759 $n=77$ cells from 4 mice, Isolated 4.837 ± 4.406 $n=92$ from 5 mice (mean \pm
514 standard deviation). Mann-Whitney test, $p< 0.0001$.

515 G Quantification of the number of *Edn3* expressing *Pecam1* positive endothelial cells. Grouped
516 0.5463 ± 0.01586 $n=5$ mice, Isolated 0.3674 ± 0.02163 $n=5$ mice (mean \pm standard error). Mann-
517 Whitney test, $p=0.0079$.

518

519 **Figure 3 - figure supplement 1 – Conditional EDNRB knock out does not affect oligodendrocyte**
520 **generation or myelin sheath length.**

521 A Representative Images of *Ednrb* mRNA expressing *Olig2* mRNA positive oligodendroglia.

522 B Ratio of CC1 positive oligodendrocytes over total population of Olig2 positive oligodendroglia. Wild
523 type 0.2086 ± 0.01087 n=5 mice, EDNRB CKO 0.2003 ± 0.0248 n=5 mice (mean \pm standard error).

524 C Number of CC1 and Olig2 positive oligodendrocytes. Wild type 1626 ± 170.6 n=5 mice, EDNRB CKO
525 1419 ± 220.5 n=5 mice (mean \pm standard error).

526 D Number Olig2 positive oligodendroglia. Wild type 7737 ± 903.8 n=5 mice, EDNRB CKO 7565 ± 1239
527 n=5 mice (mean \pm standard error).

528 E Mean myelin sheath length formed by oligodendrocytes per mouse. Wild type $46.10 \mu\text{m} \pm 2.485$
529 n=7 mice, EDNRB CKO $49.64 \mu\text{m} \pm 4.688$ n=4 mice (mean \pm standard error).

530 F Frequency distribution of myelin sheath lengths.

531 G Distance travelled by mice during 5 minutes of exploration of the social interaction assay. Wild
532 type 15.48 meters ± 3.326 n=12 mice, EDNRB CKO 17.62 meters ± 3.677 n=9 mice (mean \pm standard
533 deviation).

534 H Maximum speed travelled by mice during 5 minutes of exploration of the social interaction assay.
535 Wild type 0.2433 ± 0.04117 n=12 mice, EDNRB CKO 0.2748 meters ± 0.05095 n=9 mice (mean \pm
536 standard deviation).

537

538 **Figure 5 - figure supplement 1 – Global loss of EDNRB increases the number of oligodendrocytes in**
539 **the zebrafish spinal cord.**

540 A Representative images of MBP positive oligodendrocytes in the zebrafish spinal cord.

541 B Oligodendrocyte cell numbers in the dorsal tract: EDNRB Het 20.23 ± 5.639 , EDNRB Hom $21.21 \pm$
542 7.138 , ventral tract: EDNRB Het 39.09 ± 7.157 , EDNRB Hom 45.47 ± 7.09 and total: EDNRB Het 59.32
543 ± 9.766 , EDNRB Hom 66.79 ± 11.73 . EDNRB Het n=22 , EDNRB Hom n=14. T-test, Ventral p=0.0119,
544 Total p=0.0463.

545

546 **Figure 5 - figure supplement 2 - Global loss of EDNRB reduces the number of myelin sheath formed**
547 **by zebrafish oligodendrocytes.**

548 A Pooled data for number of myelin sheaths formed by zebrafish oligodendrocytes. Wild Type $11.9 \pm$
549 3.726 n=20 cells, EDNRB Het 11.44 ± 1.999 n=16 cells, EDNRB Hom 8.19 ± 2.994 n=21 cells from 4
550 experiments, (mean \pm standard deviation). 1-way ANOVA.

551 B Pooled data for mean myelin sheath length formed by zebrafish oligodendrocytes. Wild Type 28.45
552 ± 6.8 n=20 cells, EDNRB Het 33.04 ± 8.629 n=16 cells, EDNRB Hom 32.65 ± 7.098 n=21 from 4
553 experiments, (mean \pm standard deviation). 1-way ANOVA.

554 C Frequency distribution of myelin sheath length.

555

556 **Figure 5 - figure supplement 3 – Protein kinase C epsilon activation does not affect myelin sheath**
557 **length.**

558 A Mean myelin sheath lengths formed by oligodendrocytes in microfiber cultures. Control $16.87 \mu\text{m}$
559 ± 0.7932 , FR $16.42 \mu\text{m} \pm 1.176$ n=3-4 (mean \pm standard error).

560 B Pooled data for number myelin sheath length formed by zebrafish oligodendrocytes. EDNRB Het
561 29.62 ± 8.685 n=20 cells, EDNRB Hom 28.27 ± 7.242 n=41 from, EDNRB Het + FR 236924 $25.86 \pm$
562 10.25 n=21 cells, EDNRB Hom + FR 236924 26.48 ± 8.951 n=19 cells (mean \pm standard deviation).

563

564 **Figure 6 - figure supplement 1 – Intranasal administration of EDNRB agonist BQ3020 does not**
565 **affect myelin sheath length.**

566 A Distance travelled by mice during 5 minutes of exploration of the social interaction assay. Saline
567 17.48 meters \pm 2.697 n=12 mice, BQ3020 17.13 meters \pm 35.209 n=17 mice (mean \pm standard
568 deviation).

569 B Maximum speed travelled by mice during 5 minutes of exploration of the social interaction assay.
570 Saline 0.2769 \pm 0.03276 n=12 mice, BQ3020 0.2773 meters \pm 0.05085 n=17 mice (mean \pm standard
571 deviation).

572 C Mean myelin sheath length formed by oligodendrocytes per mouse. Saline 59.38 μ m \pm 4.831 n=28
573 cells from 4 mice, BQ3020 53.98 μ m \pm 5.748 n=28 cells from 4 mice (mean \pm standard deviation). D
574 Frequency distribution of myelin sheath lengths.

575

576 **Figure 6 - figure supplement 2 – Proposed model for how EDNRB regulates myelin sheath number.**

577 A Summary of results from paper. In a social environment, EDN from the vasculature increases
578 myelin sheath number in the medial prefrontal cortex, influencing sociability. In social isolation
579 vascular EDN production is reduced, leading to a decreased number of myelin sheaths formed by
580 oligodendrocytes and reduced sociability. Oligodendroglial knock out of EDNRB reduces the number
581 of myelin sheaths formed by oligodendrocytes and reduced sociability.

582 B Proposed hypothesis for how EDN signalling links neuronal activity to increased myelination and
583 thus support of active axons. 1. Increased local neuronal activity signals to the vasculature to
584 increase blood flow to the active area 2. The increased blood flow stimulates EDN production from
585 endothelial cells 3. Increased EDN levels leads to the formation of more myelin sheaths by
586 oligodendrocytes. Figures created with Biorender.

587

588 **Supplementary file 1 – Antibody array of phosphorylation events downstream of EDNRB.**

589 Wild type mouse oligodendrocytes were starved for 4-5 hours in media devoid of supplementation
 590 and then treated for 15 minutes with either vehicle or BQ3020 (100 ng/mL). For each antibody the
 591 background intensity was subtracted, dye signal normalised and an average calculated of the
 592 duplicate spots. The ratio was calculated of binding to the phosphorylated amino acids vs the
 593 binding to the non-modified regions of the protein for each molecule, calculating this for both
 594 control and BQ3020 treated cells. The fold change in phosphorylation for each targeted amino acid
 595 was generated by comparing BQ3020 to vehicle. For selection a fold change of greater than 2 and
 596 less than 0.5 was set as the cut-off. Antibody array was performed once – one cell lysate per
 597 condition.

598

599 **Key Resources Table**

Key Resources Table				
Reagent type (species) or resource	Designation	Source or reference	Identifiers	Additional information
Genetic reagent (M. musculus)	Ednrb flox/flox	The university of Edinburgh, Bagnall et al., 2006, Ge et al., 2006		
Genetic reagent (M. musculus)	Pdgfra-cre	Jackson labs	#013148	
Genetic reagent (D. rerio)	Rse Tlf802	Frohnhofer et al., 2013, Krauss et al., 2014		

Genetic reagent (D. rerio)	Tg(mbp:EGFP)	The University of Edinburgh, Almeida et al., 2011		
Antibody	Mouse monoclonal anti CNPase	Atlas	AMAb91072	1:2000
Antibody	Rat monoclonal anti MBP	Serotec	MCA409S	1:250
Antibody	Rat monoclonal anti PECAM1	BD Pharmingen	550274	1:100
Antibody	Rabbit monoclonal anti S100 β	Thermo	MA5-12969	1:100
Antibody	Rabbit monoclonal anti IBA1	Abcam	ab178846	1:500
Antibody	Rabbit polyclonal anti Laminin	Abcam	ab11575	1:300
Antibody	Rabbit polyclonal anti OLIG2	Millipore	ab9610	1:100
Antibody	Mouse monoclonal anti CC1	Abcam	ab16794	1:300

Antibody	Mouse monoclonal anti GAPDH	Millipore	MAB374	1:1000
Antibody	Mouse monoclonal anti Beta actin	Abcam	ab 8226	1:1000
Antibody	Rabbit polyclonal anti , Phospho-PKCε S729	Abcam	88241	1:1000
Commercial assay, kit	Phospho-explorer antibody array	Full Moon Biosystems,	Phospho-explorer array (PEX100)	
Sequence-based reagent	<i>Edn1</i>	Advanced Cell Diagnostics	435221	
Sequence-based reagent	<i>Edn2</i>	Advanced Cell Diagnostics	418221	
Sequence-based reagent	<i>Edn3</i>	Advanced Cell Diagnostics	Custom made	
Sequence-based reagent	<i>Pecam1</i>	Advanced Cell Diagnostics	316721-C3	
Sequence-based reagent	<i>Olig2</i>	Advanced Cell Diagnostics	447091	
Sequence-based reagent	<i>Ednrb</i>	Advanced Cell Diagnostics	473801	
Peptide, recombinant protein	BQ3020	Tocris	1189	100 ng/mL

Chemical compound, drug	BQ788	Tocris	1500	100 ng/mL
Chemical compound, drug	FR236924	Tocris	0373	25 μ M
Other	Microfibers	The Electrospinning company		1-2 micro diameter poly-l-lactic acid
Software, algorithm	Any-maze software	http://www.anymaze.co.uk/		
Software, algorithm	ImageJ	https://imagej.nih.gov/ij/		
Software, algorithm	Graphpad Prism	https://www.graphpad.com/scientific-software/prism/		

600

601

602 **Materials and Methods**

603 ***Mice***

604 Animal husbandry and experiments were performed under UK Home Office project licenses issued
605 under the Animals (Scientific Procedures) Act. *Ednrb*^{fl^{ox}/fl^{ox}} (Bagnall et al., 2006, Ge et al., 2006) were
606 generously provided by Professor David Webb and Professor Yuri Kotelevtsev (Edinburgh University)
607 where exons 3 and 4 are flanked with Cre-LoxP sites. Homozygous mice for the EDNRB floxed allele
608 were crossed to *Pdgfra*-cre mice obtained from Jackson laboratories (013148). Offspring were then
609 backcrossed to create mice Heterozygous for the floxed allele and carriers for the Cre transgene.
610 Experimental mice were obtained by crossing animals heterozygous for the floxed *Ednrb* allele and
611 carriers of the Cre transgene generating both *Ednrb* wild type control and *Ednrb* floxed homozygous
612 mice in the same litters. Mice were genotyped by transnetyx and confirmed as a CKO by performing

613 RNAScope for *Ednrb* (described below) Mice of each genotype were used at the ages and in the
614 numbers stated in the Results. For the social isolation experiments, postnatal day 21 male mice were
615 either group housed in a regular social environment, containing 3 – 5 mice, or in isolation, for 2
616 weeks.

617 **Sociability Test**

618 At postnatal day 35 mice were allowed to freely explore an open field arena for 5 minutes containing
619 two identical wire mesh containers. One container housed an unrelated male wild type mouse of a
620 similar age, while the other remained empty. Mice were allowed to explore the arena for 5 minutes
621 and the duration of time during which the mouse of interest came within 2.5 cm of either container
622 was automatically recorded using Any-maze software. Speed and distance travelled were also
623 recorded by the software. In all tests, mice were assessed with the experimenter blind to genotype.

624 **Intranasal Administration**

625 Mice were given brief isoflurane inhalation anaesthesia before being held upside down. Using a
626 pipette, 5 μ L of either saline or 1 μ g BQ3020 (Tocris - 1189) in saline was placed on either nostril. This
627 was repeated twice daily (9am and 5pm) from postnatal day 21 to postnatal day 31.

628 **Antibodies**

629 CNPase Atlas AMAb91072 (1:2000), MBP Serotec MCA409S (1:250), PECAM1 BD Pharmingen 550274
630 (1:100), S100 β Thermo MA5-12969 (1:100), IBA1 Abcam ab178846 (1:500), Laminin Abcam ab11575
631 (1:300), Olig2 Millipore AB9610 (1:100), CC1 Abcam ab16794 (1:300).

632 **Immunofluorescence Staining - Cryosections**

633 Animals were intracardially perfused with 4% PFA (wt/vol; Sigma) in PBS, after which brains were
634 post-fixed overnight and then cryoprotected in sucrose prior to embedding in OCT and storage at
635 -80°C . Brains were cryosectioned coronally at a thickness of 16 μm using a Thermo cryostat and
636 mounted onto Superfrost Plus slides. Sections were blocked for 1 hour at room temperature in 10%

637 goat serum, 0.1% triton in PBS. Primary antibodies were incubated in block solution at 4°C overnight.
638 Sections were washed with PBS for 3x15 minutes at room temperature and stained using species-
639 specific Alexa fluorophore-conjugated antibodies in block solution for 1 hour at room temperature.
640 Sections were washed in PBS for a further 3x15 minutes and stained with Hoechst for 5 minutes and
641 mounted onto slides with fluoromount G. Mouse medial prefrontal cortex was defined as the
642 infralimbic and prelimbic areas between bregma 1.7 mm and 2 mm and visual cortex bregma -3.5
643 mm and -4.5 mm.

644 **Immunofluorescence Staining - Vibratome Sections for Oligodendrocyte morphological analysis**

645 Animals were intracardially perfused with 4% PFA (wt/vol; Sigma) in PBS, after which brains were
646 post-fixed overnight and embedded in 2% low melting point agarose. Using a Leica vibratome, 100
647 µM coronal free-floating sections were cut. Sections underwent antigen retrieval in 0.05% Tween20,
648 10 mM tri-sodium citrate (pH 6.0) at 95 °C for 20 min. Sections were then blocked for 3 hours at
649 room temperature in 10% goat serum, 0.25% triton in PBS. Primary antibodies were incubated in
650 block solution at 4°C on a rocker for 24 hours. Sections were washed with PBS for 3 hours at room
651 temperature and stained using species-specific Alexa fluorophore-conjugated antibodies in block
652 solution for 4 hours at room temperature. Sections were washed in PBS for a further 3 hours and
653 stained with Hoechst for 20 minutes and mounted onto slides with fluoromount G. Sections were
654 analysed with the experimenter blind to experimental condition and/or genotype as below.

655 To analyse oligodendrocyte number 10 fields of 40x magnification were taken from 2 100 µm
656 sections per mouse of cortical layer II/III or layer V using a SP8 confocal microscope. CNP positive,
657 Olig2 and CC1 cells were counted.

658 To analyse oligodendrocyte morphology, random areas of the medial prefrontal cortex layer II/III
659 were imaged at 63x magnification using an SP8 confocal microscope. 7 individual CNP positive
660 oligodendrocytes per mouse, each with all myelin sheaths present within the 100 µm section as
661 assessed by following each process from the cell body and ensuring none exited the section, were

662 imaged using a z step size of 0.5 μm . Analysis was performed using an ImageJ plugin – simple neurite
663 tracer (Longair et al., 2011).

664 **RNAScope In situ Hybridisation**

665 Cryosections (cut as above) were processed as recommended by Advanced Cell Diagnostics. Briefly
666 sections were dried overnight at 60°C, after which they were incubated at 40°C with pre-treatment 4
667 for 30 minutes before incubation with RNAScope probes for 2 hours at 40°C. RNAScope probes used
668 were; *Edn1* (435221), *Edn2* (418221), *Edn3* (custom made), *Pecam1* (316721-C3), *Olig2* (447091-
669 C2), *Ednrb* (473801). Following the RNAScope protocol, sections were stained as above.

670 For analysis, 5 random 63x areas of medial prefrontal cortex layer II/III were imaged using a SP8
671 confocal microscope. Cells positive for *Pecam1* and *Edn1/3* were counted. Sections were analysed
672 with the experimenter blind to experimental condition and/or genotype.

673 **Rat Oligodendrocyte Precursor Cell Culture**

674 Rat OPCs were prepared from mixed glial cultures as described previously (McCarthy and de Vellis,
675 1980, Bechler et al., 2015). Briefly, cortices of postnatal day 0-2 Sprague Dawley rats were dissected
676 out. The tissue was digested with 1.2 Units/mL papain, 0.1 mg/mL L-cysteine and 0.40 mg/mL DNase
677 for 1 hour at 37°C. Tissue was cultured in DMEM, 10% FCS, 1% P/S in T75 flasks, pre-coated with 5
678 $\mu\text{g}/\text{mL}$ poly-D-lysine, at a density of 1.5 brains per flask. Cells were grown at 37°C in 7.5% CO_2 with
679 medium changes every 2-3 days. After 10-12 days cells were mechanically separated on an orbital
680 shaker at 250 rpm, 37°C. Loosely attached microglia were removed by shaking for 1 hour. Further
681 shaking for 16-18 hours detached OPCs. Cell yield was counted using a haemocytometer and plated
682 in assay-dependent conditions as below.

683 **Microfiber Cultures**

684 Custom parallel-aligned microfibers were purchased from the Electrospinning Company. 1-2 micron
685 diameter poly-L-lactic acid microfibers were synthesised and suspended over plastic scaffolds fitting

686 into 12-well tissue culture plates. Microfibers were washed with 70% EtOH for 10 minutes followed
687 by coating with PDL for 1 hour at 37°C in a 12 well tissue culture plate. Microfibers were washed
688 twice with sterile water and left in preheated myelination media. 35,000 rat OPCs and 50,000 mouse
689 OPCs in myelination media (50:50 DMEM:Neurobasal Media, B27 (Invitrogen), 5 µg/mL N-acetyl
690 cysteine, and 10 ng/mL D-biotin, ITS , and modified Sato (100 µg/mL BSA fraction V, 60 ng/ml
691 Progesterone, 16 µg/ml Putrescine, 400 ng/mL Tri-iodothyroxine, 400 ng/mL L-Thyroxine; reagents
692 from Sigma-Aldrich)) were triturated to break up cell clumps and added dropwise to the microfibers.
693 Cells were left to recover for 3 days before media changing and addition of treatment, followed by
694 subsequent media changes every 3 days.

695 After 14 days of culture cells were fixed in 4% PFA for 15 minutes. To visualise myelination, cells
696 were permeabilised with 0.1% Triton-X for 10 minutes and stained with for MBP (1:250) overnight at
697 4°C followed by incubation with Alexa 488-conjugated goat ant-rat (1:1000) for 1 hour at room
698 temperature and Hoescht for 5 minutes to visualise nuclei.

699 To analyse myelination 15-30 individual myelinating oligodendrocytes from one coverslip were
700 imaged (with the experimenter blind to condition) using an SP8 confocal at 40x magnification with a
701 z-step of 0.35 µm. The same settings (laser power, gain, offset etc.) were used between coverslips.
702 ImageJ was used to analyse myelination, again with the experimenter blind to condition. A sheath
703 was defined as a continuous MBP positive wrap fully surrounding a microfiber as assessed using the
704 0.35 µm z-series. Concentric tubes were traced and the length measured. In addition the number of
705 concentric sheaths made per individual oligodendrocyte was recorded. Sheath lengths were grouped
706 into 5 µm bins and the frequency from one experiment calculated. Mean frequencies from at least 3
707 experiments were generated and plotted as a frequency distribution.

708 Drugs used: BQ3020 (100ng/mL, Tocris - 1189) in 0.03M sodium bicarbonate, BQ788 (100ng/mL,
709 Tocris - 1500) in DMSO, FR236924 (25 µM, Tocris - 0373) in DMSO.

710 **Mouse Oligodendrocyte Precursor Cell Culture**

711 Mouse OPCs were isolated from P6-P9 pups as described (Watkins et al., 2008). Ear clips were taken
712 for subsequent genotyping. Briefly, cerebral cortices were dissected, diced and dissociated into
713 single-cell suspensions gently using MACS Neural Tissue Dissociation Kit P (130-092-628). Cells were
714 resuspended in 0.2% BSA, Insulin, PBS and transferred to treated tissue culture dishes coated with
715 BSL1 (L-1100, Vector Labs) for 15 minutes twice. Cell solutions were then transferred to dishes
716 coated with anti-PDGFR α (CD140a) for 45 minutes. Solutions were aspirated and attached cells
717 washed twice with media and removed with a cell scraper. All collected cells were added to vented
718 T75 flasks and grown at 37°C 7.5 CO₂. Cells were grown in myelination media containing PDGF and
719 NT3 and changed every 2 days and supplemented daily with PDGF. After 7-9 days confluent flasks
720 were washed with PBS and then detached using TrypLE for 10 minutes at 37°C. Solutions were
721 centrifuged at 1000 rpm for 5 minutes, resuspended and counted using a haemocytometer.

722 **qPCR**

723 75,000 mouse OPCs were cultured on pre-coated PDL 6 well plates for 2 days. RNA was extracted
724 from cells using a Qiagen RNeasy mini kit. RNA was then converted to cDNA libraries using a
725 SuperScript® First-Strand Synthesis System. Sybr green qPCR was performed using primers either
726 bought from Qiagen or designed at 0.5 μ M. qPCR was performed on a LightCycler 480 II. CT values
727 from designed primers were normalised against GAPDH purchased from Qiagen.

728 **Full Moon Phospho-Explorer Antibody Array**

729 Processing of the phospho-explorer array (PEX100) was performed following the Full Moon
730 Biosystems guidelines. OPCs were immunopanned from wildtype mice and expanded in the
731 presence of PDGF. Upon confluency, OPCs were differentiated through supplementation of CNTF,
732 NT3 and T3. After 2 days of differentiation cells were starved for 4-5 hours in media devoid of
733 supplementation to remove stimulation from the media and then treated for 15 minutes with either
734 vehicle or BQ3020 (100 ng/mL). Cells were lysed in RIPA buffer containing protease and phosphatase

735 inhibitors (Calbiochem – 539134 and 524621) and processed for the array as recommended by Full
736 Moon Biosystems.

737 Briefly, proteins present in the lysates were biotinylated through incubation with biotin. Chips were
738 blocked using milk and biotinylated protein lysates were washed over. Binding of the individual
739 proteins to each antibody spot on the array was assessed through fluorescent labelling with a dye-
740 labelled streptavidin read using an Innopsys 710-IR scanner and analysed using Mapix software.

741 For each antibody the background intensity was subtracted, dye signal normalised and an average
742 calculated of the duplicate spots. The ratio was calculated of binding to the phosphorylated amino
743 acids vs the binding to the non-modified regions of the protein for each molecule, calculating this for
744 both control and BQ3020 treated cells. The fold change in phosphorylation for each targeted amino
745 acid was generated by comparing BQ3020 to vehicle. For selection a fold change of greater than 2
746 and less than 0.5 was set as the cut-off.

747 Antibody array was performed once – one cell lysate per condition.

748 **Western Blot**

749 For western blot analysis, 9 cm treated plastic tissue culture dishes were coated with PDL for either
750 1 hour at 37°C or overnight at room temperature. 1 million OPCs were added in myelination media
751 to coated plates. After 3 days in culture, oligodendrocytes were starved from media
752 supplementation through incubation with DMEM and 1% P/S only for 4-5 hours. Fresh starvation
753 media was then added containing either vehicle control, BQ3020 (100 ng/mL) or FR236924 (25 µM).
754 After 10 minutes cells were lysed and scraped into RIPA buffer with protease and phosphatase
755 inhibitors (Calbiochem – 539134 and 524621) for 10 minutes on ice. Lysates were spun at 16,000 g
756 for 10 minutes and supernatants retained.

757 Protein concentration was estimated using a BCA assay kit and loaded into precast protein gels with
758 a protein marker of known molecular weights. Gels were ran at 60 volts for 30 minutes and then

759 increased to 100 volts for 1 hour. Protein was transferred from the gels to nitrocellulose membranes
760 pre-treated with methanol at 400 mA for 2 hours on ice. Membranes were blocked in 4% BSA in TBS-
761 0.1% Tween for 40 minutes and incubated with primary antibodies (GAPDH Millipore MAB374, Beta-
762 actin Abcam ab82226, Phospho-PKC ϵ S729 Abcam 88241) overnight at 4°C on an orbital shaker.
763 Membranes were washed in TBS-Tween for 30 minutes and incubated with species specific
764 secondary horseradish peroxidase antibodies at room temperature for 1 hour. Membranes were
765 washed for a further 30 minutes and incubated with ECL2 for 5 minutes. Blots were detected using a
766 Licor scanner. Subsequent western blots were performed using the same membranes following
767 removal of bound antibodies through incubation with stripping buffer for 15 minutes.

768 **Zebrafish**

769 Animal husbandry and experiments were maintained in accordance with UK Home Office guideline.
770 The following zebrafish lines were used: Wild type WIK and AB, Tg(mbp:EGFP) and EDNRB Hom (Rse
771 tLF802) (Frohnhofer et al., 2013, Krauss et al., 2014). Rse zebrafish contain a point mutation in the
772 *ednrba* gene at amino acid 163 where glutamine is substituted for lysine. This mutation creates a
773 restriction site for the enzyme PstI. Touchdown PCR was performed using a light cycler. To
774 distinguish between wild type and homozygous mutants, the PCR product was incubated with
775 restriction enzyme PstI for 3 hours at 37°C and run on a 2% agarose TAE gel. Wild type DNA remains
776 uncut at 363 bp whereas homozygous DNA generates 2 similar sized bands of 187 and 176 bp.
777 Rse Homozygous mutants were crossed to the stable transgenic line Tg(mbp:EGFP) expressing EGFP
778 in all oligodendrocytes previously generated in the Lyons lab (Almeida et al., 2011). 5 dpf larval
779 zebrafish were embedded in 1.3% low melting point agarose with tricane. Lateral images of zebrafish
780 spinal cords were taken on an Apatome2 microscope at 20x and stitched together using ZEN imaging
781 software. Using ImageJ cell counter, GFP fluorescent oligodendrocytes were counted along the
782 entire length of the dorsal and ventral spinal cord. Fish were genotyped after imaging and analysis –
783 experimenters were therefore blinded to genotype during the data acquisition.

784 Offspring of the paired mating of either Rse heterozygotes or Rse heterozygotes to Rse homozygotes
785 were subject to single oligodendrocyte analysis. Single oligodendrocytes were labelled using the
786 mbp:EGFP-CAAX plasmid developed within the Lyons lab (Almeida et al., 2011). In brief, plasmid
787 DNA generated above for the mbp:EGFP transgenic line was adapted through the addition of the 4
788 amino acid CAAX motif therefore anchoring GFP to membranes of oligodendrocytes and myelin
789 sheaths. Mosaic fish were generated by injecting fertilised eggs with 1 nL of a solution of 12.5 ng/ μ L
790 mbp:EGFP-CAAX plasmid DNA and 12.5 ng/ μ L tol2 transposase mRNA between the 1-8 cell stage.
791 Transposase mRNA was produced using an Ambion message machine kit SP6 from pre-digested
792 DNA. Injections were performed using pulled glass needles using gas to force out a precise volume,
793 measured prior to injection in a drop of mineral oil on a calibration slide. 4 dpf larval zebrafish were
794 screened for fluorescent cells and embedded in 1.3% low melting point agarose with tricane. Lateral
795 images of individual cells were taken on a Zeiss LSM710 confocal. Analysis was performed using
796 ImageJ. GFP fluorescent sheaths longer than 5 μ m were traced and the length measured. The
797 number of sheaths made by individual oligodendrocytes was recorded and the mean sheath length
798 was calculated per oligodendrocyte. Fish were genotyped after imaging and analysis - experimenters
799 were therefore blinded to genotype during the data acquisition.

800 For the experiments asking whether a protein kinase C agonist would rescue myelination defects in
801 the Rse Homozygous mutants, injected fish were treated with either 1%DMSO or 10 μ M FR236924 in
802 DMSO at 3 dpf for 24 hours before image acquisition.

803 **Statistics**

804 All analysis of cell counts and myelination and were performed on ImageJ blind to condition using a
805 filename randomiser macro. Data is presented showing standard deviations to show the variability,
806 or standard error of the mean when averaged data calculated as a mean per animal or per culture
807 was used for each n. Statistical analysis was performed using GraphPad Prism software. Data was
808 tested for normality using a Kolmogorov–Smirnov test. When data fitted a normal distribution

809 parametric t-tests and 1-way ANOVA, with Tukey's post hoc, were used. Where data did not meet
810 normal distribution non-parametric Mann-Whitney U tests and Kruskal-Wallis tests, with Dunns post
811 hoc, were used.

812

813 References

- 814 BAGNALL, A. J., KELLAND, N. F., GULLIVER-SLOAN, F., DAVENPORT, A. P., GRAY, G. A., YANAGISAWA,
815 M., WEBB, D. J. & KOTELEVTSSEV, Y. V. 2006. Deletion of endothelial cell endothelin B
816 receptors does not affect blood pressure or sensitivity to salt. *Hypertension*, 48, 286-93.
- 817 BARABAN, M., MENSCH, S. & LYONS, D. A. 2016. Adaptive myelination from fish to man. *Brain Res*,
818 1641, 149-161.
- 819 BECHLER, M. E., BYRNE, L. & FFRENCH-CONSTANT, C. 2015. CNS Myelin Sheath Lengths Are an
820 Intrinsic Property of Oligodendrocytes. *Curr Biol*.
- 821 CROWE, T. P., GREENLEE, M. H. W., KANTHASAMY, A. G. & HSU, W. H. 2018. Mechanism of
822 intranasal drug delivery directly to the brain. *Life Sci*, 195, 44-52.
- 823 DANCU, M. B., BERARDI, D. E., VANDEN HEUVEL, J. P. & TARBELL, J. M. 2004. Asynchronous shear
824 stress and circumferential strain reduces endothelial NO synthase and cyclooxygenase-2 but
825 induces endothelin-1 gene expression in endothelial cells. *Arterioscler Thromb Vasc Biol*, 24,
826 2088-94.
- 827 DUNCAN, I. D., RADCLIFF, A. B., HEIDARI, M., KIDD, G., AUGUST, B. K. & WIERENGA, L. A. 2018. The
828 adult oligodendrocyte can participate in remyelination. *Proc Natl Acad Sci U S A*, 115,
829 E11807-E11816.
- 830 ETXEBERRIA, A., HOKANSON, K. C., DAO, D. Q., MAYORAL, S. R., MEI, F., REDMOND, S. A., ULLIAN, E.
831 M. & CHAN, J. R. 2016. Dynamic Modulation of Myelination in Response to Visual Stimuli
832 Alters Optic Nerve Conduction Velocity. *J Neurosci*, 36, 6937-48.
- 833 FOSTER, A. Y., BUJALKA, H. & EMERY, B. 2019. Axoglial interactions in myelin plasticity: Evaluating
834 the relationship between neuronal activity and oligodendrocyte dynamics. *Glia*, 67, 2038-
835 2049.
- 836 FREEMAN, S. A., DESMAZIÈRES, A., SIMONNET, J., GATTA, M., PFEIFFER, F., AIGROT, M. S.,
837 RAPPENEAU, Q., GUERREIRO, S., MICHEL, P. P., YANAGAWA, Y., BARBIN, G., BROPHY, P. J.,
838 FRICKER, D., LUBETZKI, C. & SOL-FOULON, N. 2015. Acceleration of conduction velocity
839 linked to clustering of nodal components precedes myelination. *Proc Natl Acad Sci U S A*,
840 112, E321-8.
- 841 FROHNHÖFER, H. G., KRAUSS, J., MAISCHEIN, H. M. & NÜSSLEIN-VOLHARD, C. 2013. Iridophores and
842 their interactions with other chromatophores are required for stripe formation in zebrafish.
843 *Development*, 140, 2997-3007.
- 844 FÜNFSCILLING, U., SUPPLIE, L. M., MAHAD, D., BORETIUS, S., SAAB, A. S., EDGAR, J., BRINKMANN,
845 B. G., KASSMANN, C. M., TZVETANOVA, I. D., MÖBIUS, W., DIAZ, F., MEIJER, D., SUTER, U.,
846 HAMPRECHT, B., SEREDA, M. W., MORAES, C. T., FRAHM, J., GOEBBELS, S. & NAVE, K. A.
847 2012. Glycolytic oligodendrocytes maintain myelin and long-term axonal integrity. *Nature*,
848 485, 517-21.
- 849 GE, Y., BAGNALL, A., STRICKLETT, P. K., STRAIT, K., WEBB, D. J., KOTELEVTSSEV, Y. & KOHAN, D. E.
850 2006. Collecting duct-specific knockout of the endothelin B receptor causes hypertension
851 and sodium retention. *Am J Physiol Renal Physiol*, 291, F1274-80.
- 852 GERAGHTY, A. C., GIBSON, E. M., GHANEM, R. A., GREENE, J. J., OCAMPO, A., GOLDSTEIN, A. K., NI,
853 L., YANG, T., MARTON, R. M., PAŞCA, S. P., GREENBERG, M. E., LONGO, F. M. & MONJE, M.

2019. Loss of Adaptive Myelination Contributes to Methotrexate Chemotherapy-Related Cognitive Impairment. *Neuron*, 103, 250-265.e8.

GIBSON, E. M., NAGARAJA, S., OCAMPO, A., TAM, L. T., WOOD, L. S., PALLEGAR, P. N., GREENE, J. J., GERAGHTY, A. C., GOLDSTEIN, A. K., NI, L., WOO, P. J., BARRES, B. A., LIDDELOW, S., VOGEL, H. & MONJE, M. 2019. Methotrexate Chemotherapy Induces Persistent Tri-glial Dysregulation that Underlies Chemotherapy-Related Cognitive Impairment. *Cell*, 176, 43-55.e13.

GIBSON, E. M., PURGER, D., MOUNT, C. W., GOLDSTEIN, A. K., LIN, G. L., WOOD, L. S., INEMA, I., MILLER, S. E., BIERI, G., ZUCHERO, J. B., BARRES, B. A., WOO, P. J., VOGEL, H. & MONJE, M. 2014. Neuronal activity promotes oligodendrogenesis and adaptive myelination in the mammalian brain. *Science*, 344, 1252304.

HAMMOND, T. R., GADEA, A., DUPREE, J., KERNINON, C., NAIT-OUESMAR, B., AGUIRRE, A. & GALLO, V. 2014. Astrocyte-derived endothelin-1 inhibits remyelination through notch activation. *Neuron*, 81, 588-602.

HAMMOND, T. R., MCELLIN, B., MORTON, P. D., RAYMOND, M., DUPREE, J. & GALLO, V. 2015. Endothelin-B Receptor Activation in Astrocytes Regulates the Rate of Oligodendrocyte Regeneration during Remyelination. *Cell Rep*, 13, 2090-7.

HILL, R. A., LI, A. M. & GRUTZENDLER, J. 2018. Lifelong cortical myelin plasticity and age-related degeneration in the live mammalian brain. *Nat Neurosci*, 21, 683-695.

HINES, J. H., RAVANELLI, A. M., SCHWINDT, R., SCOTT, E. K. & APPEL, B. 2015. Neuronal activity biases axon selection for myelination in vivo. *Nat Neurosci*, 18, 683-9.

HORIUCHI, M., SUZUKI-HORIUCHI, Y., AKIYAMA, T., ITOH, A., PLEASURE, D., CARSTENS, E. & ITOH, T. 2017. Differing intrinsic biological properties between forebrain and spinal oligodendroglial lineage cells. *J Neurochem*, 142, 378-391.

HUGHES, E. G., ORTHMANN-MURPHY, J. L., LANGSETH, A. J. & BERGLES, D. E. 2018. Myelin remodeling through experience-dependent oligodendrogenesis in the adult somatosensory cortex. *Nat Neurosci*, 21, 696-706.

ISHIBASHI, T., DAKIN, K. A., STEVENS, B., LEE, P. R., KOZLOV, S. V., STEWART, C. L. & FIELDS, R. D. 2006. Astrocytes promote myelination in response to electrical impulses. *Neuron*, 49, 823-32.

JÄKEL, S., AGIRRE, E., MENDANHA FALCÃO, A., VAN BRUGGEN, D., LEE, K. W., KNUESEL, I., MALHOTRA, D., FFRENCH-CONSTANT, C., WILLIAMS, A. & CASTELO-BRANCO, G. 2019. Altered human oligodendrocyte heterogeneity in multiple sclerosis. *Nature*, 566, 543-547.

KOUDELKA, S., VOAS, M. G., ALMEIDA, R. G., BARABAN, M., SOETAERT, J., MEYER, M. P., TALBOT, W. S. & LYONS, D. A. 2016. Individual Neuronal Subtypes Exhibit Diversity in CNS Myelination Mediated by Synaptic Vesicle Release. *Curr Biol*.

KOUGIOUMTZIDOU, E., SHIMIZU, T., HAMILTON, N. B., TOHYAMA, K., SPRENGEL, R., MONYER, H., ATTWELL, D. & RICHARDSON, W. D. 2017. Signalling through AMPA receptors on oligodendrocyte precursors promotes myelination by enhancing oligodendrocyte survival. *Elife*, 6.

KRAUSS, J., FROHNHÖFER, H. G., WALDERICH, B., MAISCHEIN, H. M., WEILER, C., IRION, U. & NÜSSLEIN-VOLHARD, C. 2014. Endothelin signalling in iridophore development and stripe pattern formation of zebrafish. *Biol Open*, 3, 503-9.

LEE, S., LEACH, M. K., REDMOND, S. A., CHONG, S. Y., MELLON, S. H., TUCK, S. J., FENG, Z. Q., COREY, J. M. & CHAN, J. R. 2012a. A culture system to study oligodendrocyte myelination processes using engineered nanofibers. *Nat Methods*, 9, 917-22.

LEE, Y., MORRISON, B. M., LI, Y., LENGACHER, S., FARAH, M. H., HOFFMAN, P. N., LIU, Y., TSINGALIA, A., JIN, L., ZHANG, P. W., PELLERIN, L., MAGISTRETTI, P. J. & ROTHSTEIN, J. D. 2012b. Oligodendroglia metabolically support axons and contribute to neurodegeneration. *Nature*, 487, 443-8.

904 LIU, J., DIETZ, K., DELOYHT, J. M., PEDRE, X., KELKAR, D., KAUR, J., VIALOU, V., LOBO, M. K., DIETZ, D.
905 M., NESTLER, E. J., DUPREE, J. & CASACCIA, P. 2012. Impaired adult myelination in the
906 prefrontal cortex of socially isolated mice. *Nat Neurosci*, 15, 1621-3.

907 LONGAIR, M. H., BAKER, D. A. & ARMSTRONG, J. D. 2011. Simple Neurite Tracer: open source
908 software for reconstruction, visualization and analysis of neuronal processes. *Bioinformatics*,
909 27, 2453-4.

910 MAKINODAN, M., ROSEN, K. M., ITO, S. & CORFAS, G. 2012. A critical period for social experience-
911 dependent oligodendrocyte maturation and myelination. *Science*, 337, 1357-60.

912 MARQUES, S., VAN BRUGGEN, D., VANICHKINA, D. P., FLORIDDIA, E. M., MUNGUBA, H., VÄREMO, L.,
913 GIACOMELLO, S., FALCÃO, A. M., MEIJER, M., BJÖRKLUND, Å., HJERLING-LEFFLER, J., TAFT, R.
914 J. & CASTELO-BRANCO, G. 2018. Transcriptional Convergence of Oligodendrocyte Lineage
915 Progenitors during Development. *Dev Cell*.

916 MCCARTHY, K. D. & DE VELLIS, J. 1980. Preparation of separate astroglial and oligodendroglial cell
917 cultures from rat cerebral tissue. *J Cell Biol*, 85, 890-902.

918 MCKENZIE, I. A., OHAYON, D., LI, H., DE FARIA, J. P., EMERY, B., TOHYAMA, K. & RICHARDSON, W. D.
919 2014. Motor skill learning requires active central myelination. *Science*, 346, 318-22.

920 MEI, F., FANCY, S. P., SHEN, Y. A., NIU, J., ZHAO, C., PRESLEY, B., MIAO, E., LEE, S., MAYORAL, S. R.,
921 REDMOND, S. A., ETXEBERRIA, A., XIAO, L., FRANKLIN, R. J., GREEN, A., HAUSER, S. L. &
922 CHAN, J. R. 2014. Micropillar arrays as a high-throughput screening platform for therapeutics
923 in multiple sclerosis. *Nat Med*, 20, 954-60.

924 MENSCH, S., BARABAN, M., ALMEIDA, R., CZOPKA, T., AUSBORN, J., EL MANIRA, A. & LYONS, D. A.
925 2015. Synaptic vesicle release regulates myelin sheath number of individual
926 oligodendrocytes in vivo. *Nat Neurosci*, 18, 628-30.

927 MEYER, N., RICHTER, N., FAN, Z., SIEMONSMEIER, G., PIVNEVA, T., JORDAN, P., STEINHÄUSER, C.,
928 SEMTNER, M., NOLTE, C. & KETTENMANN, H. 2018. Oligodendrocytes in the Mouse Corpus
929 Callosum Maintain Axonal Function by Delivery of Glucose. *Cell Rep*, 22, 2383-2394.

930 MITEW, S., GOBIUS, I., FENLON, L. R., MCDUGALL, S. J., HAWKES, D., XING, Y. L., BUJALKA, H.,
931 GUNDLACH, A. L., RICHARDS, L. J., KILPATRICK, T. J., MERSON, T. D. & EMERY, B. 2018.
932 Pharmacogenetic stimulation of neuronal activity increases myelination in an axon-specific
933 manner. *Nat Commun*, 9, 306.

934 PANDIT, M. M., INSCHO, E. W., ZHANG, S., SEKI, T., ROHATGI, R., GUSELLA, L., KISHORE, B. & KOHAN,
935 D. E. 2015. Flow regulation of endothelin-1 production in the inner medullary collecting
936 duct. *Am J Physiol Renal Physiol*, 308, F541-52.

937 SAAB, A. S., TZVETAVONA, I. D., TREVISIOL, A., BALTAN, S., DIBAJ, P., KUSCH, K., MÖBIUS, W.,
938 GOETZE, B., JAHN, H. M., HUANG, W., STEFFENS, H., SCHOMBURG, E. D., PÉREZ-SAMARTÍN,
939 A., PÉREZ-CERDÁ, F., BAKHTIARI, D., MATUTE, C., LÖWEL, S., GRIESINGER, C., HIRRLINGER, J.,
940 KIRCHHOFF, F. & NAVE, K. A. 2016. Oligodendroglial NMDA Receptors Regulate Glucose
941 Import and Axonal Energy Metabolism. *Neuron*.

942 SAMPAIO-BAPTISTA, C. & JOHANSEN-BERG, H. 2017. White Matter Plasticity in the Adult Brain.
943 *Neuron*, 96, 1239-1251.

944 SAMPAIO-BAPTISTA, C., KHRAPITCHEV, A. A., FOXLEY, S., SCHLAGHECK, T., SCHOLZ, J., JBABDI, S.,
945 DELUCA, G. C., MILLER, K. L., TAYLOR, A., THOMAS, N., KLEIM, J., SIBSON, N. R.,
946 BANNERMAN, D. & JOHANSEN-BERG, H. 2013. Motor skill learning induces changes in white
947 matter microstructure and myelination. *J Neurosci*, 33, 19499-503.

948 SCAFIDI, J., HAMMOND, T. R., SCAFIDI, S., RITTER, J., JABLONSKA, B., RONCAL, M., SZIGETI-BUCK, K.,
949 COMAN, D., HUANG, Y., MCCARTER, R. J., HYDER, F., HORVATH, T. L. & GALLO, V. 2014.
950 Intranasal epidermal growth factor treatment rescues neonatal brain injury. *Nature*, 506,
951 230-4.

952 SCHOLZ, J., KLEIN, M. C., BEHRENS, T. E. & JOHANSEN-BERG, H. 2009. Training induces changes in
953 white-matter architecture. *Nat Neurosci*, 12, 1370-1.

954 SEIDL, A. H., RUBEL, E. W. & BARRÍA, A. 2014. Differential conduction velocity regulation in ipsilateral
955 and contralateral collaterals innervating brainstem coincidence detector neurons. *J Neurosci*,
956 34, 4914-9.

957 SEIDL, A. H., RUBEL, E. W. & HARRIS, D. M. 2010. Mechanisms for adjusting interaural time
958 differences to achieve binaural coincidence detection. *J Neurosci*, 30, 70-80.

959 SUMINAITE, D., LYONS, D. A. & LIVESEY, M. R. 2019. Myelinated axon physiology and regulation of
960 neural circuit function. *Glia*, 67, 2050-2062.

961 TIMMLER, S. & SIMONS, M. 2019. Grey matter myelination. *Glia*.

962 TOMASSY, G. S., BERGER, D. R., CHEN, H. H., KASTHURI, N., HAYWORTH, K. J., VERCELLI, A., SEUNG,
963 H. S., LICHTMAN, J. W. & ARLOTTA, P. 2014. Distinct profiles of myelin distribution along
964 single axons of pyramidal neurons in the neocortex. *Science*, 344, 319-24.

965 TSAI, H. H., NIU, J., MUNJI, R., DAVALOS, D., CHANG, J., ZHANG, H., TIEN, A. C., KUO, C. J., CHAN, J. R.,
966 DANEMAN, R. & FANCY, S. P. 2016. Oligodendrocyte precursors migrate along vasculature in
967 the developing nervous system. *Science*, 351, 379-84.

968 WALSHE, T. E., FERGUSON, G., CONNELL, P., O'BRIEN, C. & CAHILL, P. A. 2005. Pulsatile flow
969 increases the expression of eNOS, ET-1, and prostacyclin in a novel in vitro coculture model
970 of the retinal vasculature. *Invest Ophthalmol Vis Sci*, 46, 375-82.

971 WATKINS, T. A., EMERY, B., MULINYAWE, S. & BARRES, B. A. 2008. Distinct stages of myelination
972 regulated by gamma-secretase and astrocytes in a rapidly myelinating CNS coculture system.
973 *Neuron*, 60, 555-69.

974 XIAO, L., OHAYON, D., MCKENZIE, I. A., SINCLAIR-WILSON, A., WRIGHT, J. L., FUDGE, A. D., EMERY, B.,
975 LI, H. & RICHARDSON, W. D. 2016. Rapid production of new oligodendrocytes is required in
976 the earliest stages of motor-skill learning. *Nat Neurosci*, 19, 1210-7.

977 YAMAMURO, K., YOSHINO, H., OGAWA, Y., MAKINODAN, M., TORITSUKA, M., YAMASHITA, M.,
978 CORFAS, G. & KISHIMOTO, T. 2018. Social Isolation During the Critical Period Reduces
979 Synaptic and Intrinsic Excitability of a Subtype of Pyramidal Cell in Mouse Prefrontal Cortex.
980 *Cereb Cortex*, 28, 998-1010.

981 YANAGISAWA, M., KURIHARA, H., KIMURA, S., TOMOBE, Y., KOBAYASHI, M., MITSUI, Y., YAZAKI, Y.,
982 GOTO, K. & MASAKI, T. 1988. A novel potent vasoconstrictor peptide produced by vascular
983 endothelial cells. *Nature*, 332, 411-5.

984 YEUNG, M. S. Y., DJELLOUL, M., STEINER, E., BERNARD, S., SALEHPOUR, M., POSSNERT, G., BRUNDIN,
985 L. & FRISÉN, J. 2019. Dynamics of oligodendrocyte generation in multiple sclerosis. *Nature*,
986 566, 538-542.

987 YUEN, T. J., JOHNSON, K. R., MIRON, V. E., ZHAO, C., QUANDT, J., HARRISINGH, M. C., SWIRE, M.,
988 WILLIAMS, A., MCFARLAND, H. F., FRANKLIN, R. J. & FFRENCH-CONSTANT, C. 2013.
989 Identification of endothelin 2 as an inflammatory factor that promotes central nervous
990 system remyelination. *Brain*, 136, 1035-47.

991 YUEN, T. J., SILBEREIS, J. C., GRIVEAU, A., CHANG, S. M., DANEMAN, R., FANCY, S. P., ZAHED, H.,
992 MALTEPE, E. & ROWITCH, D. H. 2014. Oligodendrocyte-encoded HIF function couples
993 postnatal myelination and white matter angiogenesis. *Cell*, 158, 383-96.

994 ZHANG, Y., CHEN, K., SLOAN, S. A., BENNETT, M. L., SCHOLZE, A. R., O'KEEFE, S., PHATNANI, H. P.,
995 GUARNIERI, P., CANEDA, C., RUDERISCH, N., DENG, S., LIDDELOW, S. A., ZHANG, C.,
996 DANEMAN, R., MANIATIS, T., BARRES, B. A. & WU, J. Q. 2014. An RNA-sequencing
997 transcriptome and splicing database of glia, neurons, and vascular cells of the cerebral
998 cortex. *J Neurosci*, 34, 11929-47.

999

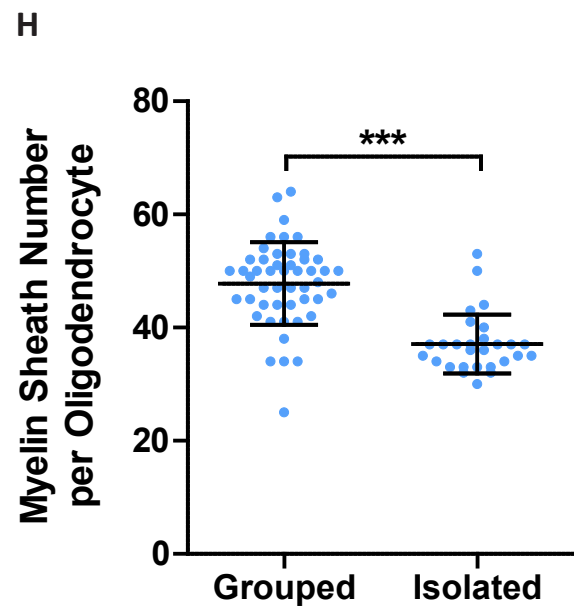
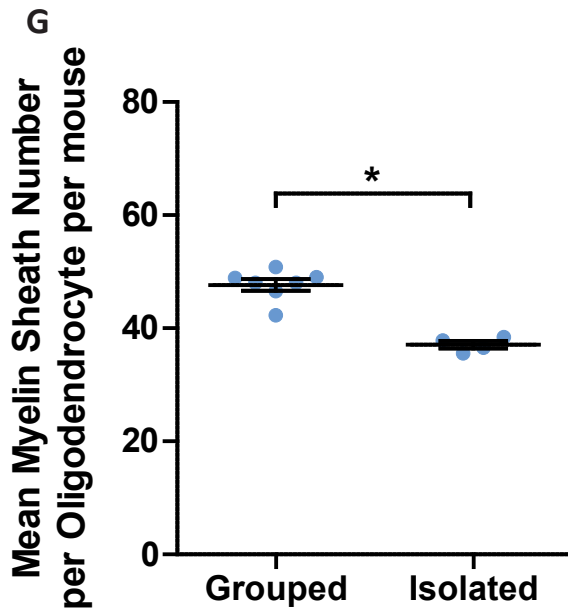
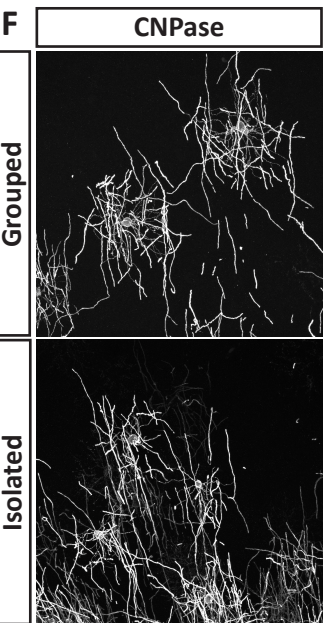
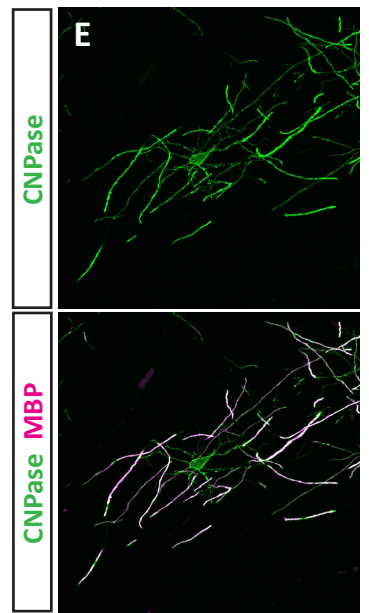
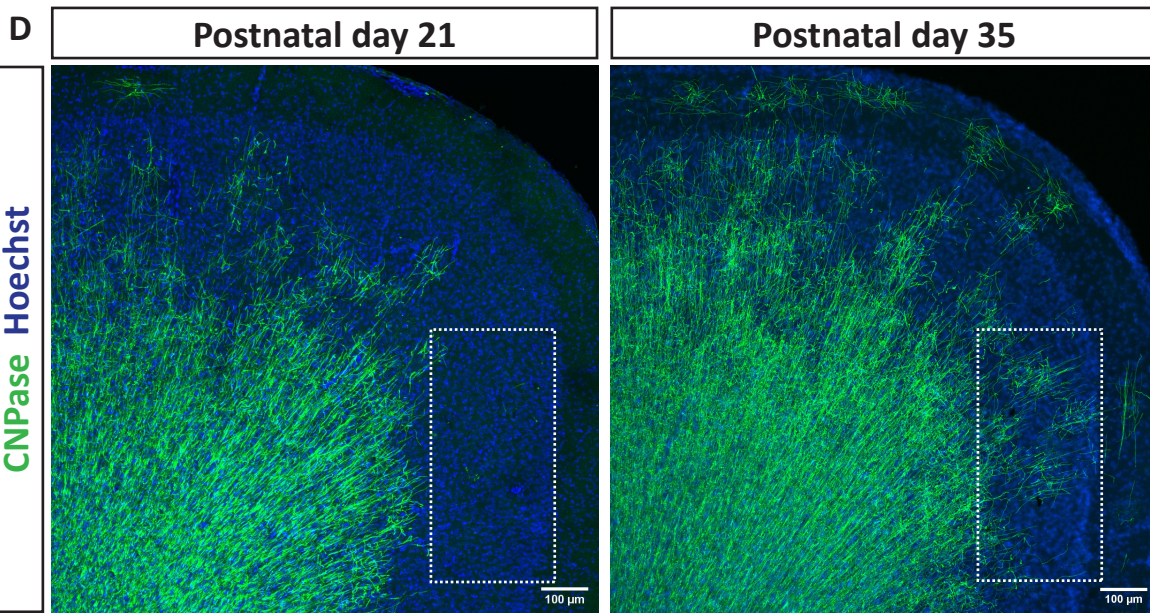
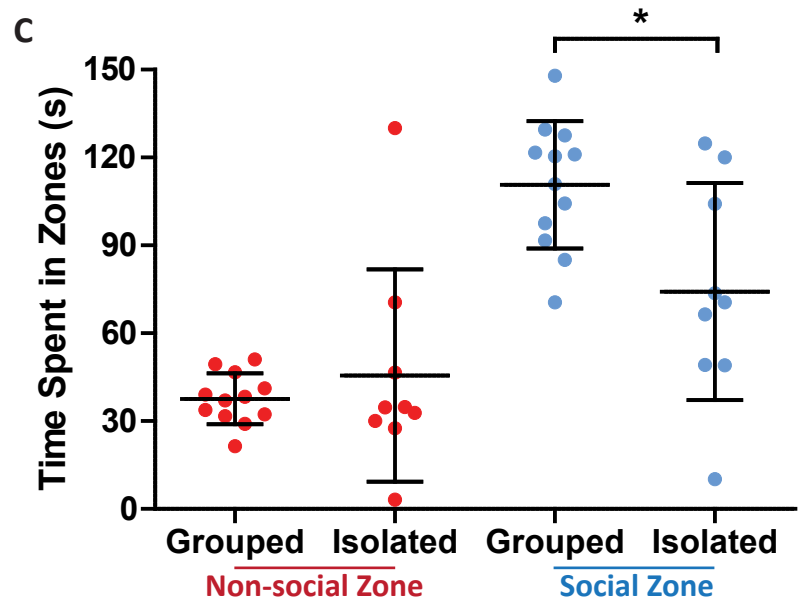
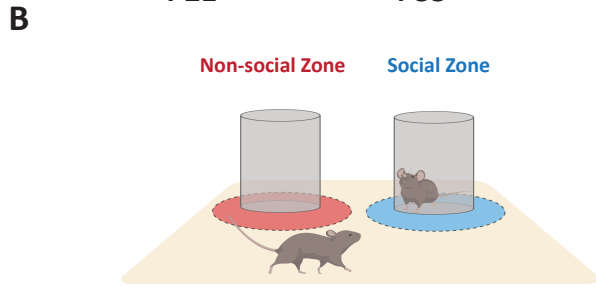
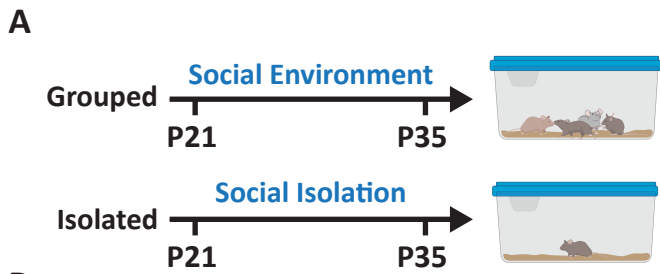
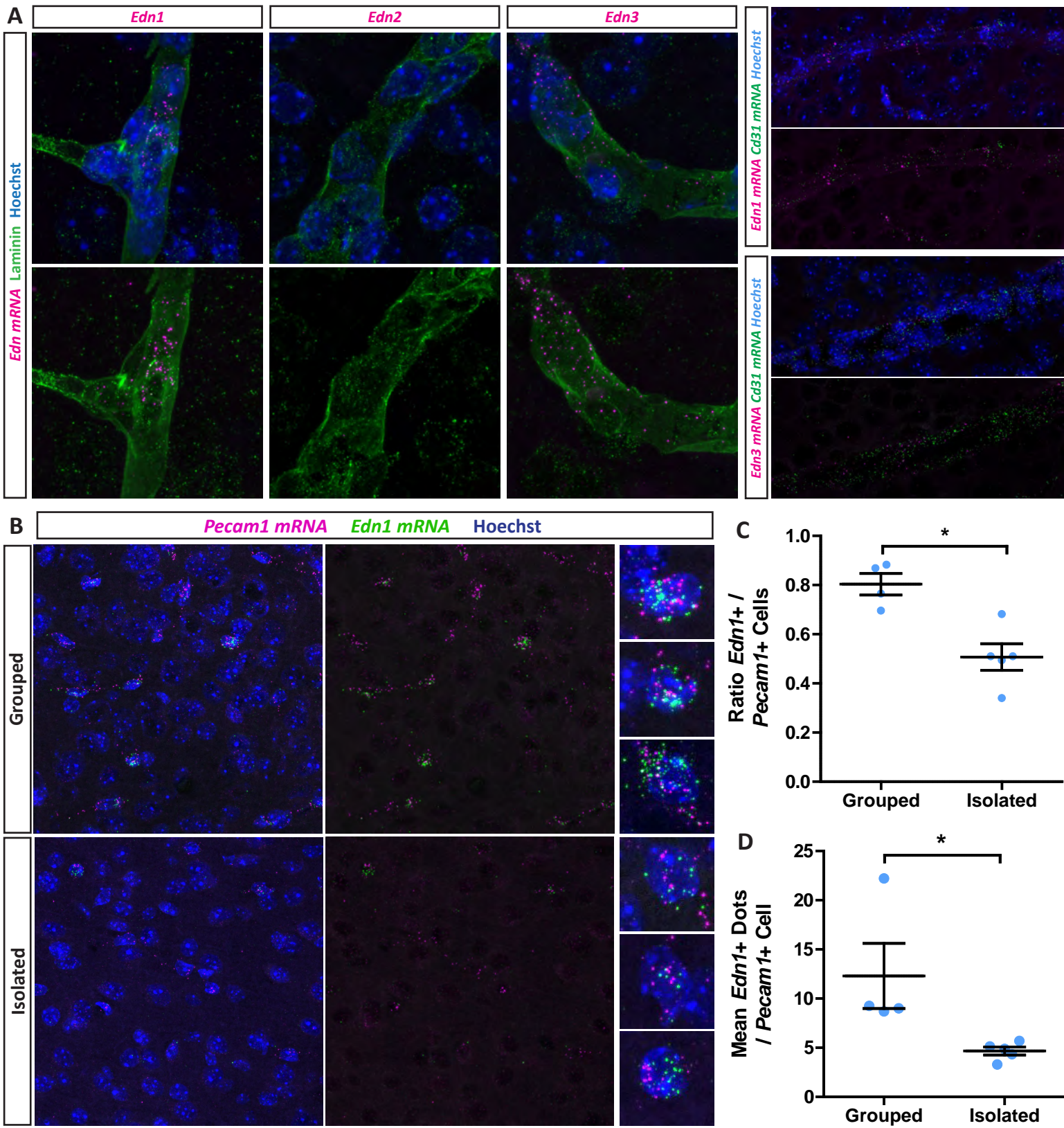
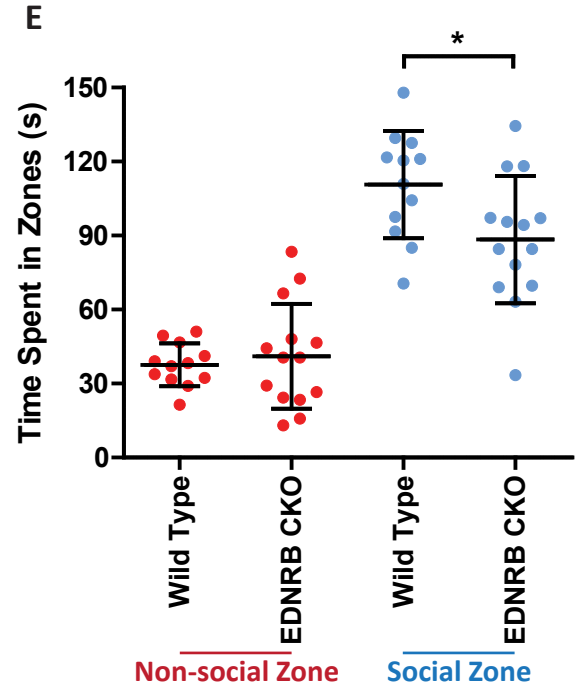
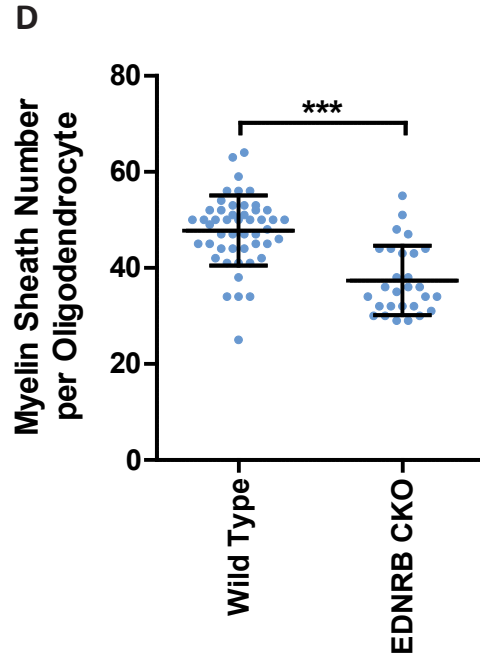
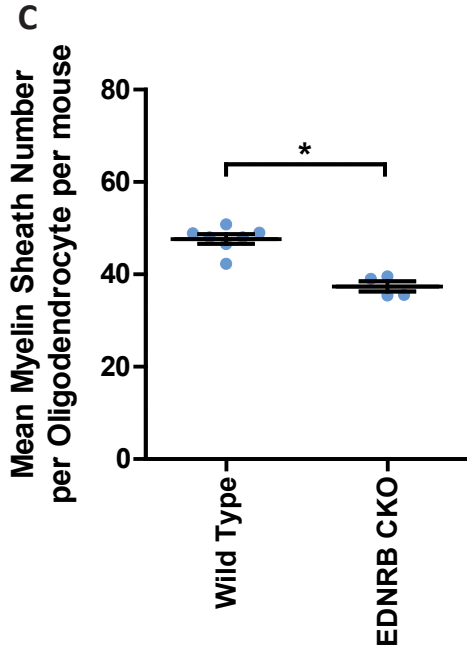
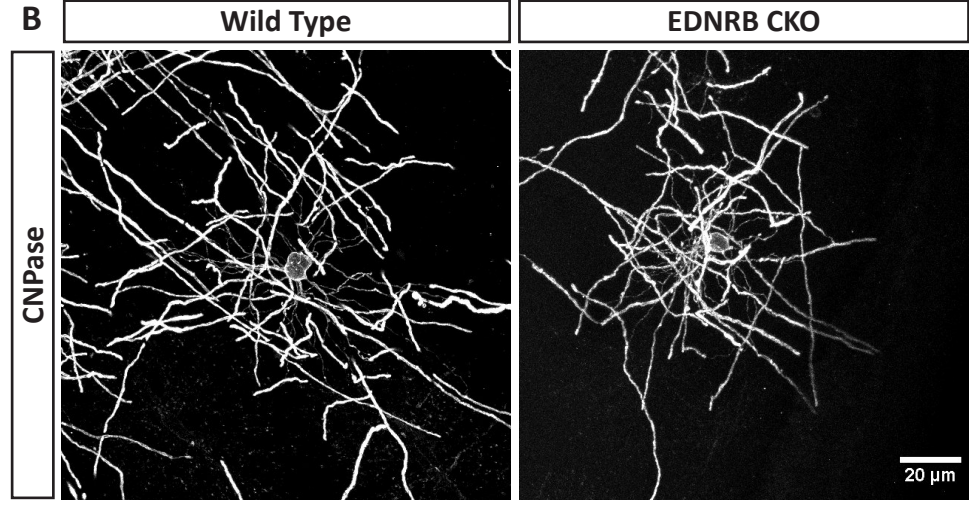
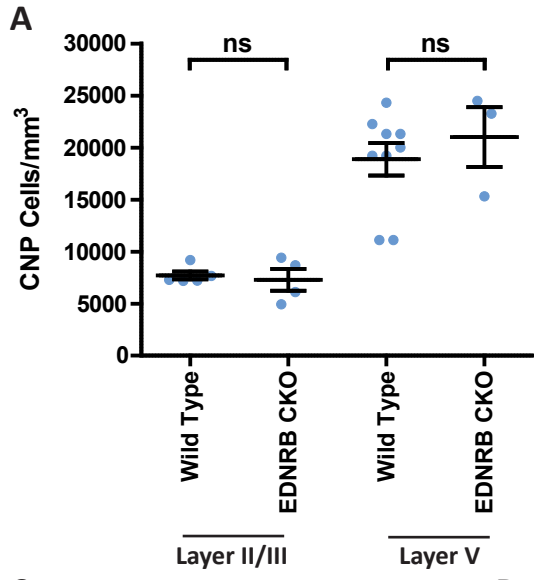
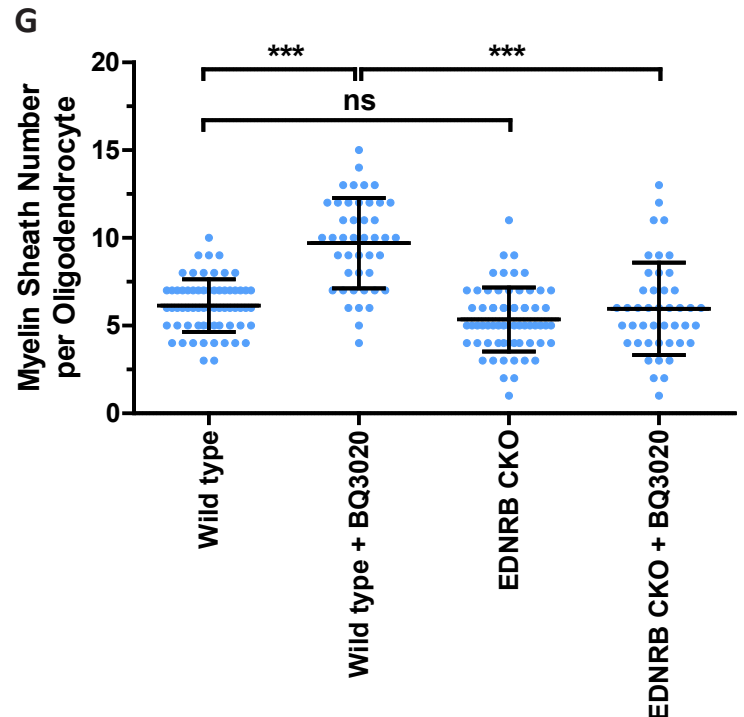
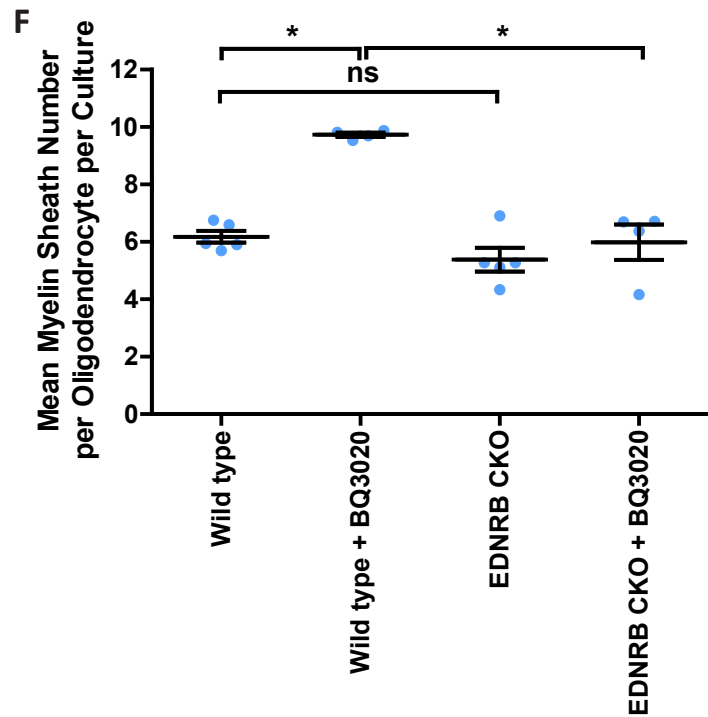
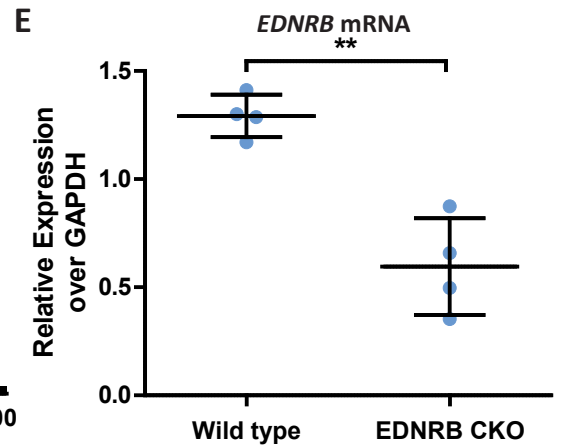
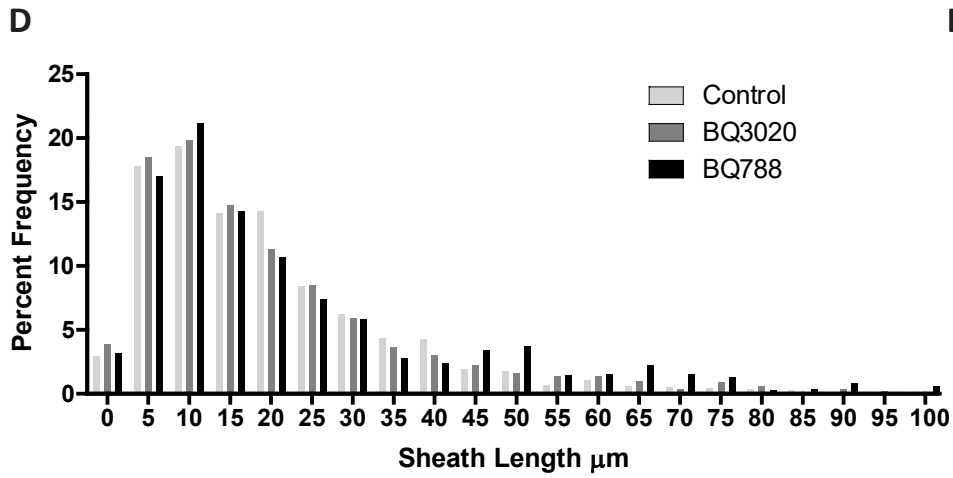
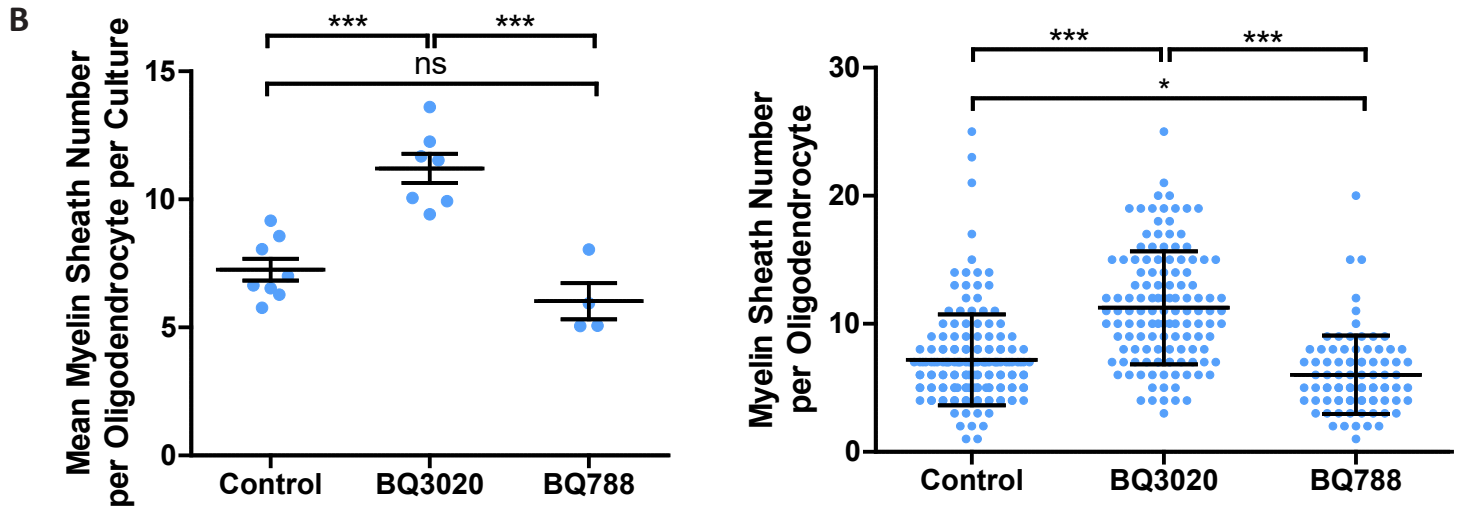
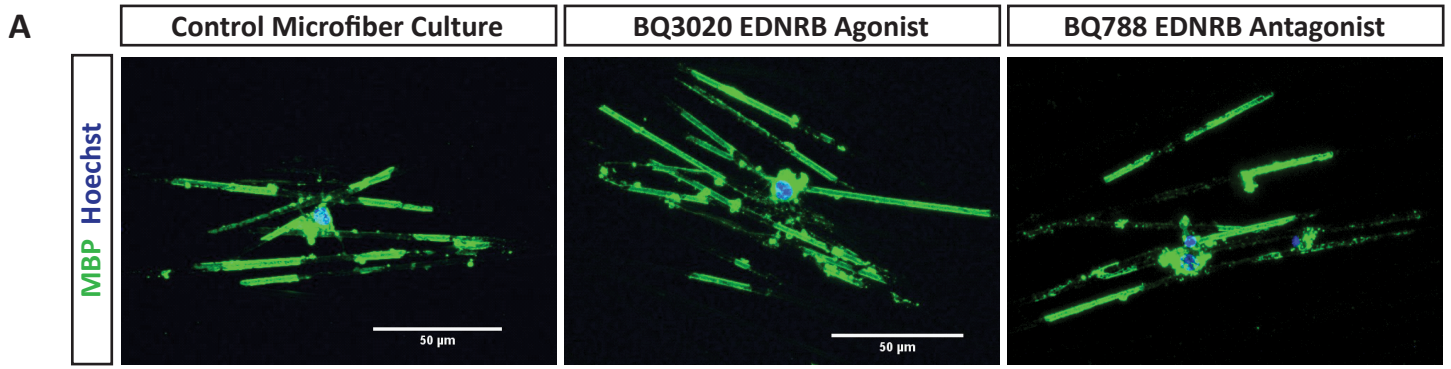
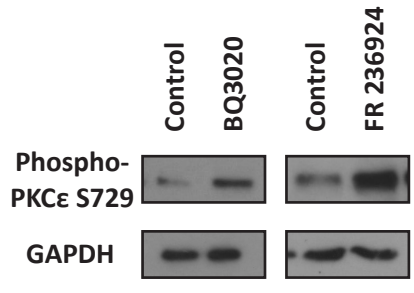
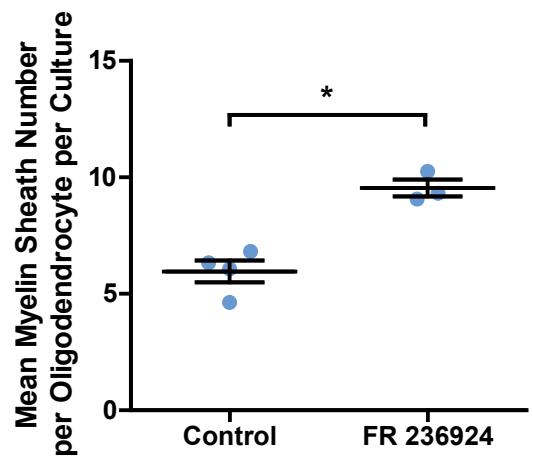
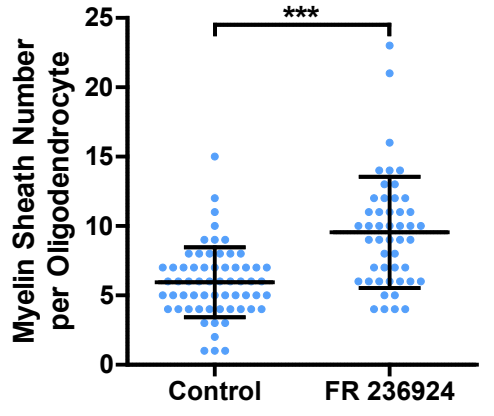
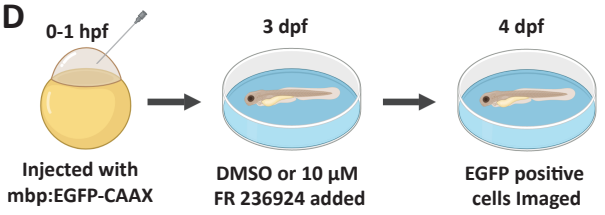
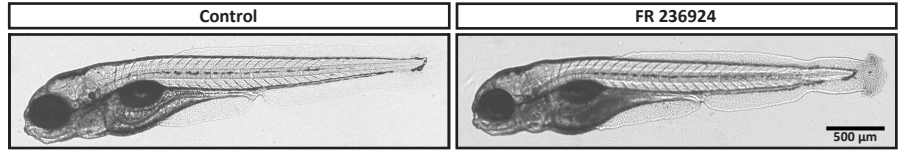
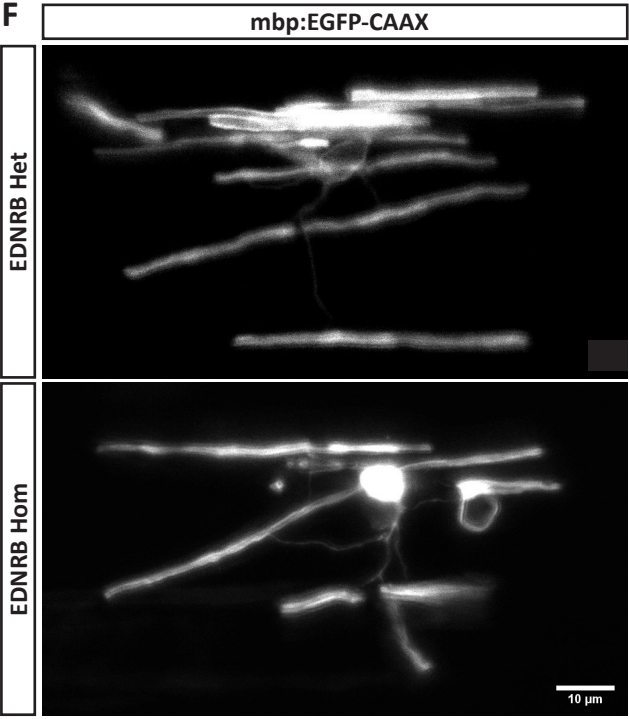


Figure 2 – Social isolation reduces vascular endothelin expression.







A**B****C****D****E****F****G**